

J-driven Dynamic Nuclear Polarization: A new mechanism for sensitizing high field solution state NMR

Maria Grazia Concilio^{1*}, *Ilya Kuprov*², *Lucio Frydman*,^{1,3*}

¹Department of Chemical and Biological Physics, Weizmann Institute of Science, Rehovot, Israel.

²School of Chemistry, University of Southampton, Southampton, UK.

³National High Magnetic Field Laboratory, Tallahassee, Florida, USA.

Keywords: dynamic nuclear polarization, biradicals, three-spin effects, radical-pair mechanism.

Highlights:

Biradicals whose electron Larmor frequencies match J_{ex} can enhance NMR signals at ≤ 30 T field.

These enhancements reach $\approx \gamma_{\text{electron}}/\gamma_{\text{nucleus}}$ efficiencies

The nuclear polarization build-ups are transient events requiring ≤ 50 ms microwave irradiation.

The efficiency is nearly independent of rotational correlation times for systems of relevance.

Abstract

Dynamic nuclear polarization (DNP) is widely used to enhance the sensitivity of nuclear magnetic resonance (NMR). Predicted by Overhauser in the 1950s, DNP is presently the method of choice for enhancing the sensitivity of high-field solid state NMR experiments performed under cryogenic conditions. In liquids, however, the efficiency of Overhauser's DNP (ODNP) decays rapidly with magnetic field B_0 and with the rotational correlation time, leading to negligible enhancements in mid- and high-field solution-state NMR experiments for all but exceptional cases. This reflects the inverse dependence that ODNP's polarization build-up rates show with the electron Larmor frequency ω_E , which become negligible for conventional liquids when $B_0 \geq 1\text{T}$. This study discusses a potential solution to this fundamental sensitivity problem, that relies on biradical species possessing inter-electron exchange couplings J_{ex} that are on the order of ω_E . It is shown based on numerical calculations as well as using Redfield's analytical relaxation theory that, when such condition is met, a microwave-driven phenomenon akin to that occurring in chemically induced dynamic nuclear polarization can happen. In it, the different relaxation properties of the biradical's singlet and triplet states when dipole coupled to the nuclear α or β states, can act as a sort of "nuclear spin filter" that will –depending on J_{ex} 's sign – transiently build up the population one nuclear spin state over the other. We refer to this new mechanism as J-driven DNP (J-DNP). Analytical and numerical derivations reveal key differences between J-DNP and ODNP –foremost among them a weak B_0 field dependence, relatively high efficiencies at low microwave powers, a slight increase in efficiency with the rotational correlation time of the biradical/nuclear triad, and a nuclear polarization build-up that, unlike what happens in ODNP and for DNP in general, is a transient event rather than a steady state.

Corresponding authors:

*maria-grazia.concilio@weizmann.ac.il

*lucio.frydman@weizmann.ac.il

1. Introduction

Low sensitivity is nuclear magnetic resonance's (NMR's) Achilles Heel: If endowed with the sensitivity of optical or mass spectroscopies, NMR could bring transformative breakthroughs to analytical, pharmaceutical and biophysical chemistries. NMR sensitivity can be enhanced by using ever higher magnetic fields, but technical problems make this a slow, expensive approach. An alternative to enhancing NMR sensitivity arises if a highly polarized reservoir, such as an electron in a stable radical, is immersed in a strong external magnetic field B_0 , and placed close to the nuclei to be detected. By irradiating the electrons near their Larmor frequency ω_E , the so-called Dynamic Nuclear Polarization (DNP) effect can then transfer the electron's polarization to the adjacent nuclei, enhancing the sensitivity of NMR experiments by ca. the ratio γ_E/γ_N of their gyromagnetic ratios; i.e., by factors ranging from 100- to 1000-fold. Predicted by Overhauser in 1953 [1] and thereafter confirmed by Carver and Slichter [2], DNP has revolutionized solid state NMR [3-6]; it has also made inroads into *in vivo* spectroscopy, based on rapid melting approaches [7, 8]. DNP, however, has not yet impacted what is arguably the widest of NMR's realm: solution-state NMR. This is due to a longstanding problem, whereby the efficiency of Overhauser's DNP (ODNP) in liquids depends on the electron-nuclear cross-relaxation rate $\sigma_{E,N}$:

$$\sigma_{E,N} \approx \frac{\gamma_E^2 \gamma_N^2 \hbar^2}{10} \left(\frac{\mu_0}{4\pi} \right)^2 \frac{\tau_C}{r_{EN}^6} \left(\frac{6}{1 + (\omega_E + \omega_N)^2 \tau_C^2} - \frac{1}{1 + (\omega_E - \omega_N)^2 \tau_C^2} \right), \quad (1)$$

which decreases dramatically with the external magnetic field B_0 . Indeed τ_C , the electron/nucleus pair rotational correlation time, is in normal liquids on the order of 10-500s ps. As at conventional NMR fields the electron's Larmor frequencies fall in the 200-1000 GHz range, the ensuing $(\omega_E \pm \omega_N)^2 \tau_C^2 > 1$ situation ends up leading to very slow transfer rates. As a result of this –and unless aided by scalar couplings that may arise for certain molecule/radical pairs [9-13]– typical electron \rightarrow ^1H ODNP enhancements drop from their maximum of $\approx 330\text{x}$ at 0.4T, to $\approx 1.001\text{x}$ at the high ≥ 7 T fields where contemporary NMR is performed [9, 14-17]. Very recently, we discussed a way to bypass ODNP's demand for substantial spectral densities at the electron Larmor frequency, based on an alternative mechanism of polarization transfer that survives at high magnetic fields. The ensuing cross-correlated (CC) DNP [18] strategy for electron \rightarrow nuclear polarization transfers, relies on a two-electron biradical which needs to fulfill numerous simultaneous requirements in order to pass its polarization to a nearby nucleus. These include a significant coincidence between the strengths of the electrons' Larmor g -anisotropy and the inter-electron dipolar coupling, between the g -anisotropies and the nuclear-electron dipolar coupling tensors, and between the two nuclear-electron dipolar anisotropies. Only if all these instances are fulfilled, and if the nuclear-electron system remains geometrically stable for long enough, can the three cross-correlated relaxation processes needed for CCDNP effect be sufficiently active, to create a net transfer of electron polarization to the nucleus under high fields and for common solution-state τ_C 's. The ensuing steady-state enhancements in nuclear polarization then approached $\approx 10\text{-}20\text{x}$, for optimal conditions.

Further investigations on the spin physics of such three-spin system have revealed an entirely new electron \rightarrow nuclear polarization transfer possibility, which we introduce in this work. The system to be treated is once again composed by two electrons and one nucleus (a proton), but unlike in CCDNP the new electron \rightarrow nuclear transfer mechanism: (i) no longer demands stringent coincidences between multiple independent coupling tensors; (ii) can lead to nuclear polarization enhancements in the 100-200x range for a wide range of B_0 fields (from below 1 to above 20 T) and of correlation times τ_C

(≈ 100 -1 ns); and (iii) does not result from a steady-state solution of the spin states upon electron saturation, but rather from transient phenomena. At the centre of this new proposal are two electrons interacting through an exchange coupling J_{ex} , whose magnitude is on the order of their electron Larmor frequency. As such electron-electron couplings can be tuned by chemical design and have been observed to range from ≈ 0 to ≥ 1 THz [19, 20], this $\omega_E \approx J_{ex}$ condition is not an unreasonable demand. Under such exchange coupling condition, we found that moderate microwave (μW) fields can lead to nearly maximal $\gamma_E/2\gamma_N$ enhancements for τ_C values in the ps-ns range –with no additional demands on the system being imposed, other than for a proximity between the biradical and the nucleus. The central role that the exchange coupling plays in this mechanism led us to call it J-driven DNP (J-DNP). The present theoretical study discusses first the existence of this mechanism based on full Liouville space numerical simulations for a variety of conditions; we then justify these numerical results based on analytical derivations stemming from Redfield’s relaxation theory [21-25]. The latter serve to highlight similarities between the roles that the electronic singlet and triplet states play in polarizing nuclei in this new DNP effect, and those played by the singlet and triplet states normally arising in chemically-induced DNP experiments like those used for enhancing the NMR signals of certain photoactive groups [26-29].

2. Features of J-driven DNP

The spin system to be considered involves a biradical –two covalently linked unpaired electrons sitting at proximate organic centres– and one proton that is nearby to these electrons. The clearest way to highlight the differences between the CCDNP and J-DNP mechanisms is by lifting the former relatively stringent demands. The two electrons were thus assumed to have identical g -tensors (these were made anisotropic for the sake of realism, even if Supporting Information 6 shows that nuclear shielding or g -anisotropies are not required to see the J-DNP enhancement). Dipolar hyperfine couplings were assumed to exist both between the electrons as well as between each electron and the proton, as defined by inter-particle distances that were assumed fixed. No electron-nuclear scalar couplings of the kind that could lead to high-field ODNP [9-13], were considered. The most important variable in the system was the isotropic inter-electron exchange coupling J_{ex} , which was modelled on the basis of trityl-based symmetric biradicals for which such couplings have been observed [19, 20]. Given trityl’s moderate g -anisotropy leading to relatively long solution-state T_{1s} and T_{2s} [30, 31] (see Supporting Information 1 for more detailed analyses on the relations between T_1 and T_2 , microwave power and rotational correlation times for trityl and bistrityl electron spins), this work derives from simulations performed using the bistrityl-inspired parameters shown in Table 1. These parameters were used to create the three-spin system rotating frame Hamiltonian, and to calculate the latter’s time-dependent evolution subject to microwave irradiation and to spin relaxation as per Redfield’s theory [21, 24]. J-DNP’s behaviour for systems with parameters that differ from those in Table 1, are discussed in Supporting Information 6.

Table 1: Biradical / proton magnetic resonance parameters used in the simulations shown in Figures 1-6. Each electron in the biradical had its parameters modelled on a trityl centre, with an inter-electron distance of 20 Å [19, 20], and the nucleus placed closer to one of the electrons. B_0 , J_{ex} and τ_c were set as described in the figures; all other coupling parameters relied on the inter-spin distances.

Parameter	Value
^1H chemical shift tensor, ppm	[5 10 20]
g -tensor ¹ for electrons 1 and 2, Bohr magneton	[2.0032 2.0032 2.0026]
^1H coordinates, [x y z], Å	[-3 0.5 1.3] (11.1 Å and 8.6 Å from the two electrons)
Electron 1 coordinates, [x y z], Å	[0 0 -9.37]
Electron 2 coordinates, [x y z], Å	[0 0 9.37]
Scalar relaxation modulation depth, GHz ²	3
Scalar relaxation modulation time, ps ²	1
Microwave saturation field $\omega_{\mu\text{w}}/2\pi$, MHz	1
Temperature, K	298

¹ Simulations used these Zeeman interaction tensors, that were then made axially symmetric along the main molecular axis (corresponding the linker connecting the two trityls).

Figure 1 shows how the isotropic inter-electron exchange coupling J_{ex} modulates the maximum achievable nuclear enhancement achievable by J-DNP, as a function of magnetic field B_0 . These plots, based on the Spinach numerical simulation package [33], predict that, for every field strength, there are two $J_{ex} = \pm(\omega_E + \omega_N)$ values for which microwave irradiation at ω_E , will lead to a nuclear enhancement that is close to the maximum achievable $\gamma_E/2\gamma_N$ ODNP value.

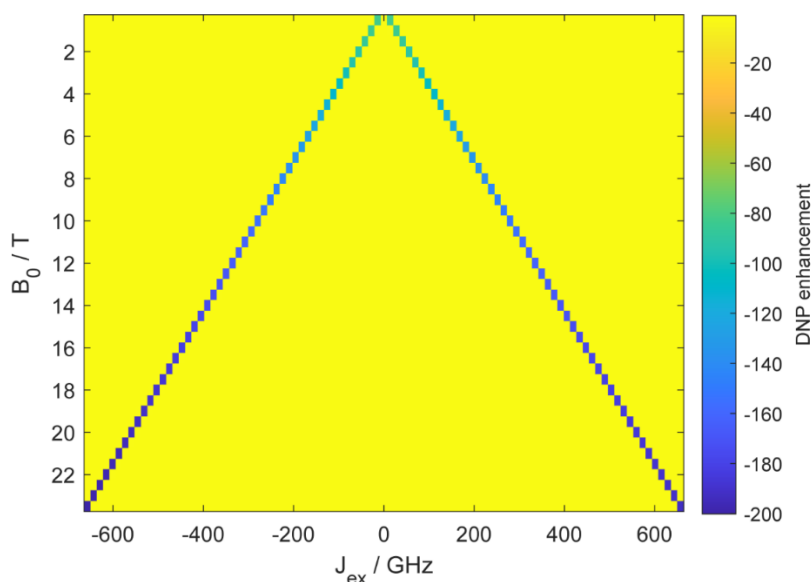


Fig. 1: Dynamic nuclear polarization enhancement achieved within 20 ms of microwave irradiation, as a function of J_{ex} and B_0 . The plots arise from time domain simulations using the three-spin site parameters given in Table 1, a biradical/nuclear rotational correlation time of 500 ps, and an on-resonance irradiation of the biradicals at their isotropic-g Larmor frequency. In this and other enhancement graphs shown in this study DNP enhancements (colorbar) are shown normalized to the thermal equilibrium nuclear polarization value at that field and temperature (i.e., DNP enhancement = 1 means no enhancement).

Unlike previously described ODNP and CCDNP enhancements, the nuclear polarization enhancements shown in Figure 1 for $J_{\text{ex}} = \pm(\omega_{\text{E}} + \omega_{\text{N}})$ conditions, are transient phenomena. This is illustrated in Figure 2, which shows this DNP enhancement's time-dependence for different rotational correlation times and B_0 magnetic fields, for spin systems with an optimally chosen $J_{\text{ex}} = (\omega_{\text{E}} + \omega_{\text{N}})$ coupling that are subject to continuous microwave irradiation. As can be seen the nuclear polarization rapidly builds up, and then decays into steady states. At low magnetic field ($B_0 = 0.5$ T) these steady-state values are higher for faster tumbling systems, whereas at the usual NMR fields used in analytical and biophysical studies (≥ 7 T), these long-term steady states are essentially identical to the Boltzmann nuclear equilibrium (data not shown). In all cases, however, substantial transient enhancements are observed after 10-50 ms of irradiation, with precise timings and maximal values that depend weakly on B_0 and τ_{C} . These behaviours are radically different from classical ODNP expectations.

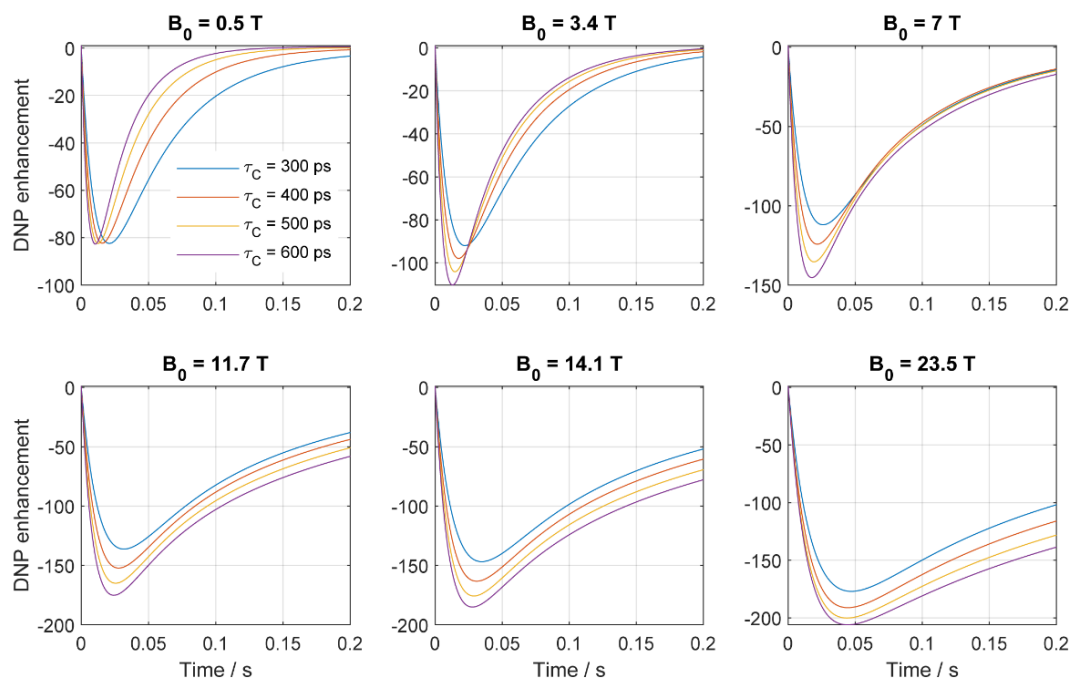


Fig. 2: Time domain simulations showing the evolution of the DNP enhancement observed under continuous microwave irradiation of the electrons, for an array of B_0 and of τ_{C} values. For all fields, the J_{ex} was set to $\omega_{\text{E}} + \omega_{\text{N}}$; other simulation parameters are as given in Table 1.

Additional differences between the behaviours of conventional ODNP and J-DNP are stressed in Figure 3, which compares expectations from a two-spin proton/electron system interacting through dipolar interactions (ODNP), and the changes arising when a second, J_{ex} -coupled electron is added in the form of a biradical with $J_{\text{ex}} = \omega_{\text{E}} + \omega_{\text{N}}$. For the electron/nucleus ODNP case the enhancement is strong if $B_0 < 0.5$ T, but decays to negligible values if $B_0 \geq 3.4$ T; this is as expected from classical theories [10, 11, 14-16]. Upon introducing a second electron in the form of a biradical, very similar steady-state values are reached for the nuclear polarization—but in the way to those steady states, there are strong transient enhancements. In fact, as illustrated in Figure 2 and in Supporting Information 6 for other kinds of systems, the nuclear enhancements associated this transient effect may improve with both higher magnetic fields and slower correlation times. These are again basic features of the J-DNP effect that differ from conventional ODNP, and whose bases are explained in the next section.

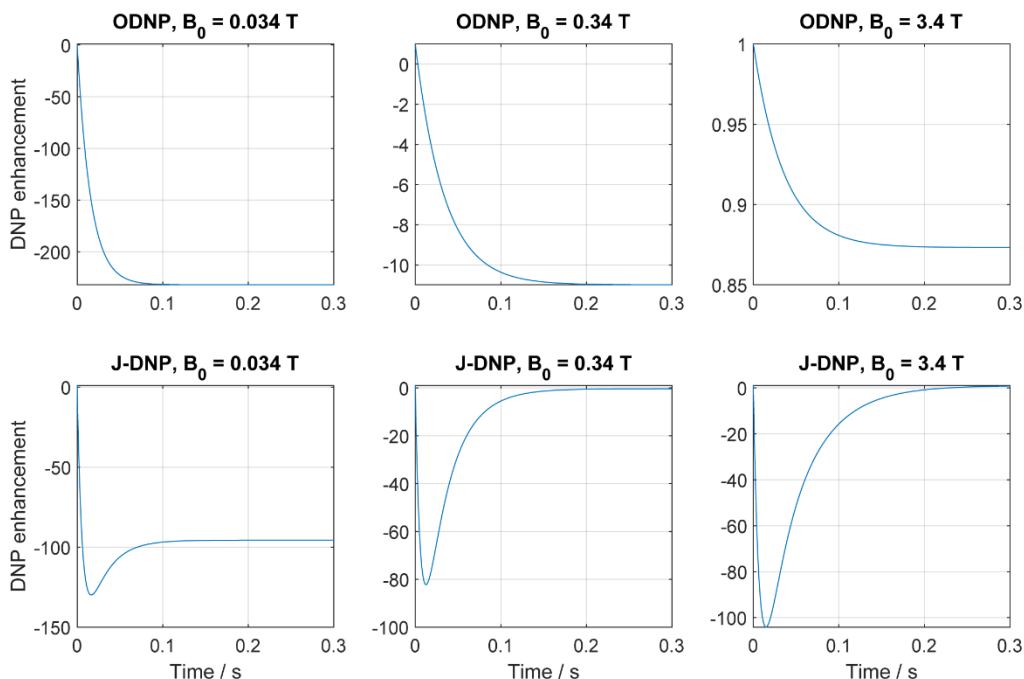


Fig. 3: Time domain simulations showing the evolution of the enhancement observed under continuous microwave irradiation of the electrons as a function of B_0 , in ODNP (top panels) and in J-DNP (bottom panels). For ODNP a monoradical with $\tau_C = 157$ ps (typical of trityl [34]) was assumed; for J-DNP a biradical with $\tau_C = 500$ ps (close to what's expected for a trityl biradical) and $J_{ex} = \omega_E + \omega_N$ was assumed. Other simulation parameters are as in the Table 1.

3. The Physics of J-driven DNP

The physics that drives the J-DNP effects summarized in Figures 1-3, are reminiscent to those arising in chemically-induced DNP (CIDNP). According to the radical pair theory [27, 28, 35], CIDNP's nuclear polarization enhancement proceeds on the basis of three processes: (i) singlet/triplet interconversions within a spin-correlated biradical system; (ii) a modulation of the rate of this interconversion depending on the magnitude and the sign of the electrons' hyperfine couplings to a nucleus, i.e., depending on whether the nuclear spin state is α or β ; and (iii) a transient action of the ensuing hyperfine-modulated triplet biradical as a "nuclear spin-state filter", biasing one of the nuclear spin-state's relaxation rate over the other. In the $J_{ex} = \pm(\omega_E + \omega_N)$ case the biradical is not photochemically or chemically produced and does not spontaneously recombine after a transient action; still, the aforementioned singlet-triplet behaviour vis-à-vis the nuclear spin once again becomes relevant, given the large size of the J_{ex} coupling the two electrons. In the J-DNP case it will be microwaves (rather than a laser) that drive the system away from the thermal equilibrium; and as in CIDNP it is essential that the nucleus be differentially hyperfine-coupled to the two electrons, for the J-DNP enhancement to occur; the effect disappears otherwise (Supporting Figure S11). It will be the differential relaxation characteristics of these singlet/triplet electronic states when facing the nuclear α or β states, that will then build up the nuclear polarization.

To translate these features into a representative mathematical description, a simplified system was considered: scalar couplings between proton and electrons were disregarded, and the two strongly-coupled electrons were assumed to have identical g-factors. In such $J_{ex} \gg \omega_{\Delta e}$ case, where $\omega_{\Delta e} = \omega_{E1} - \omega_{E2}$ is the difference between the Larmor frequency of the two electrons, the electronic

Zeeman eigenstates $|\alpha_{e1}\beta_{e2}\rangle$ and $|\beta_{e1}\alpha_{e2}\rangle$ are no longer eigenfunctions of the spin Hamiltonian. Instead, it is convenient to express the Hamiltonian in the singlet/triplet electron basis sets [6]:

$$\left\{ \begin{array}{l} |T_{+1}^{(e1e2)}\rangle = |\alpha_{e1}\alpha_{e2}\rangle, |T_0^{(e1e2)}\rangle = \frac{1}{\sqrt{2}}(|\beta_{e1}\alpha_{e2}\rangle + |\alpha_{e1}\beta_{e2}\rangle), \\ |T_{-1}^{(e1e2)}\rangle = |\beta_{e1}\beta_{e2}\rangle, |S_0^{(e1e2)}\rangle = \frac{1}{\sqrt{2}}(|\beta_{e1}\alpha_{e2}\rangle - |\alpha_{e1}\beta_{e2}\rangle) \end{array} \right\} \otimes \{|\alpha_N, \beta_N\rangle\} = \left\{ \begin{array}{l} |S_0^{(e1e2)}, \alpha\rangle, |S_0^{(e1e2)}, \beta\rangle \\ |T_0^{(e1e2)}, \alpha\rangle, |T_0^{(e1e2)}, \beta\rangle \\ |T_{\pm 1}^{(e1e2)}, \alpha\rangle, |T_{\pm 1}^{(e1e2)}, \beta\rangle \end{array} \right\} \quad (2)$$

where the direct product indicates that the $\{|\alpha_N\rangle, |\beta_N\rangle\}$ Zeeman basis is preserved for the nucleus (proton). The transformation of the three-spin rotating frame Hamiltonian from a Cartesian basis to its singlet/triplet basis can be performed using fictitious spin- $\frac{1}{2}$ operators.[36] As shown in the Supporting Information 2, this leads to the rotating frame irradiation Hamiltonian:

$$\hat{H}_{rot} = \hat{H}^{S_0T_0} + \hat{H}^{T_{+1}T_{-1}} + \hat{H}_{\mu w} \quad (3a)$$

where the term acting in the S_0T_0 space corresponds to

$$\begin{aligned} \hat{H}^{S_0T_0} = & 2\omega_{\Delta e} \left(L_X^{T_0S_0,\alpha} + L_X^{T_0S_0,\beta} \right) + A_{\Delta} \left(L_X^{T_0S_0,\alpha} - L_X^{T_0S_0,\beta} \right) + B_{\Delta} \left(L_X^{S_0T_0,\alpha\beta} + L_X^{T_0S_0,\alpha\beta} \right) + \\ & - \omega_2 \left(L_Z^{T_0S_0,\alpha} + L_Z^{T_0S_0,\beta} \right) - \omega_1 \left(\frac{\mathbf{E}^{T_0S_0,\alpha} + \mathbf{E}^{T_0S_0,\beta}}{4} \right) \end{aligned} \quad (3b)$$

the term acting in the $T_{+1}T_{-1}$ space is

$$\begin{aligned} \hat{H}^{T_{+1}T_{-1}} = & 2\omega_e \left(L_Z^{T_{\pm 1},\alpha} + L_Z^{T_{\pm 1},\beta} \right) \hat{R}_y^{T_{\pm 1}}(\theta) + \omega_N \hat{N}_Z + B_{\Sigma} \left(L_X^{T_{+1},\alpha\beta} - L_X^{T_{-1},\alpha\beta} \right) \\ & + A_{\Sigma} \left(L_Z^{T_{+1},\alpha} - L_Z^{T_{-1},\beta} \right) + \omega_1 \left(\frac{\mathbf{E}^{T_{+1},\alpha} + \mathbf{E}^{T_{-1},\beta}}{4} \right) \end{aligned} \quad (3c)$$

and $\hat{H}_{\mu w} = \omega_{\mu w}(\hat{E}_{1X} + \hat{E}_{2X})$ is the microwave irradiation operator, with $\omega_{\mu w}$ the strength of its nutation frequency. Here $\omega_{\Sigma e}$ and $\omega_{\Delta e} \sim 0$ are the sum and difference between the electron Larmor frequencies of the biradical (ω_E) and the microwave irradiation frequency; $A_{\Sigma} = A_1 + A_2$ and $A_{\Delta} = A_1 - A_2$, $B_{\Sigma} = B_1 + B_2$ and $B_{\Delta} = B_1 - B_2$ are the sum and the difference of the secular and pseudo-secular coefficients describing the hyperfine interaction, respectively; $\omega_1 = (J_{ex} + 2\mathbf{D})$ and $\omega_2 = (J_{ex} - \mathbf{D})$, where \mathbf{D} is the inter-electron dipolar interaction tensor. $\hat{R}_y^{T_{\pm 1}}(\theta)$ in Eq. (3c) is a rotation matrix about the y-axis that acts on both the α and β space; its associated $2\omega_e \left(L_Z^{T_{\pm 1},\alpha} + L_Z^{T_{\pm 1},\beta} \right) \hat{R}_y^{T_{\pm 1}}(\theta)$ term then corresponds to $\omega_e \cos(\theta) \left(L_Z^{T_{\pm 1},\alpha} + L_Z^{T_{\pm 1},\beta} \right) + \omega_e \sin(\theta) (\hat{E}_{1X} + \hat{E}_{2X})$, with $\theta = \arctan(\omega_{\mu w}/\omega_{\Sigma e})$ the angle felt by the electron's effective field, and $\omega_e = \sqrt{\omega_{\Sigma e}^2 + \omega_{\mu w}^2}$ the effective field's strength. A matrix representation of the full rotating frame Hamiltonian in Eq. (3a) can thus be written as:

	$ S_0^{(\epsilon e_2)}, \alpha\rangle$	$ T_{+1}^{(\epsilon e_2)}, \alpha\rangle$	$ T_0^{(\epsilon e_2)}, \alpha\rangle$	$ T_{-1}^{(\epsilon e_2)}, \alpha\rangle$	$ S_0^{(\epsilon e_2)}, \beta\rangle$	$ T_{+1}^{(\epsilon e_2)}, \beta\rangle$	$ T_0^{(\epsilon e_2)}, \beta\rangle$	$ T_{-1}^{(\epsilon e_2)}, \beta\rangle$
$ S_0^{(\epsilon e_2)}, \alpha\rangle$	$-\frac{\omega_1}{4} - \frac{\omega_2}{2} + \frac{\omega_N}{2}$	0	$\frac{A_{\Delta} + \omega_{\Delta\epsilon}}{2}$	0	0	0	$\frac{B_{\Delta}}{2}$	0
$ T_{+1}^{(\epsilon e_2)}, \alpha\rangle$	0	$\frac{A_{\Delta} + \omega_1 + \omega_2 \cos(\theta) + \frac{\omega_N}{2}}{2}$	$\frac{\omega_2 \sin(\theta)}{\sqrt{2}}$	0	0	$\frac{B_{\Delta}}{2}$	0	0
$ T_0^{(\epsilon e_2)}, \alpha\rangle$	$\frac{A_{\Delta} + \omega_{\Delta\epsilon}}{2}$	$\frac{\omega_2 \sin(\theta)}{\sqrt{2}}$	$-\frac{\omega_1}{4} + \frac{\omega_2}{2} + \frac{\omega_N}{2}$	$\frac{\omega_2 \sin(\theta)}{\sqrt{2}}$	0	0	0	0
$ T_{-1}^{(\epsilon e_2)}, \alpha\rangle$	0	0	$\frac{B_{\Delta}}{2}$	0	0	0	$-\frac{A_{\Delta} + \omega_{\Delta\epsilon}}{2}$	0
$ S_0^{(\epsilon e_2)}, \beta\rangle$	0	0	0	0	$-\frac{\omega_1}{4} - \frac{\omega_2}{2} - \frac{\omega_N}{2}$	0	$-\frac{A_{\Delta} + \omega_2 - \omega_N}{2}$	0
$ T_{+1}^{(\epsilon e_2)}, \beta\rangle$	0	$\frac{B_{\Delta}}{2}$	0	0	0	$-\frac{A_{\Delta} + \omega_1 + \omega_2 \cos(\theta) - \frac{\omega_N}{2}}{2}$	$\frac{\omega_2 \sin(\theta)}{\sqrt{2}}$	0
$ T_0^{(\epsilon e_2)}, \beta\rangle$	$\frac{B_{\Delta}}{2}$	0	0	0	$-\frac{A_{\Delta} + \omega_{\Delta\epsilon}}{2}$	$-\frac{\omega_1}{4} + \frac{\omega_2}{2} - \frac{\omega_N}{2}$	$\frac{\omega_2 \sin(\theta)}{\sqrt{2}}$	0
$ T_{-1}^{(\epsilon e_2)}, \beta\rangle$	0	0	0	$-\frac{B_{\Delta}}{2}$	0	0	$\frac{\omega_2 \sin(\theta)}{\sqrt{2}}$	$\frac{A_{\Delta} + \omega_1 - \omega_2 \cos(\theta) - \frac{\omega_N}{2}}{2}$

Notice that in this Hamiltonian, microwave-related terms act solely within the triplet manifold mixing the $T_{\pm 1}^{(e1e2)}$ and $T_0^{(e1e2)}$ states, but do not involve the $S_0^{(e1e2)}$ singlet. The latter, however, is not isolated: it gets connected to $T_0^{(e1e2)}$ via the difference in secular hyperfine couplings with the nucleus A_Δ . Should there be an inequivalence in the electronic g 's of the two electrons, that would also provide such off-diagonal connection. (Additional simulations –not shown– demonstrate that the pseudosecular terms are not essential for describing the J-DNP effect).

With this Hamiltonian as starting point, Liouville-space time domain simulations were performed to propagate the equation of motion:

$$\frac{\partial}{\partial t} \hat{\rho}(t) = -i\hat{L}\hat{\rho}(t), \quad \hat{L} = \hat{H}_{rot} + i\hat{R}, \quad O(t) = \langle \hat{O} | \hat{\rho}(t) \rangle \quad (7)$$

where $\hat{\rho}(t)$ is the state vector containing the information about the system, and \hat{L} is the Liouvillian containing the rotating frame Hamiltonian superoperator with the internal plus microwave interactions (described in the Supporting Information 2), and an \hat{R} relaxation superoperator accounting for the stochastic fluctuations in all anisotropic interactions. The latter was computed according to the Bloch-Redfield-Wangsness relaxation theory [21, 37], leading to Redfield's relaxation matrix elements. These were obtained using both analytical [23] and numerical [24, 25] means, and they included all possible longitudinal, transverse and cross-correlated pathways. Since the spin system was considered at room temperature the DiBari – Levitt thermalization was used [38]. Considering that the exchange coupling has the same order of magnitude of the electron Larmor frequency, simulations took into account a scalar relaxation of the first kind [32], that was incorporated into the relaxation superoperator. This, however, did not have an effect on the enhancement, since in the $\omega_{\Delta e} \rightarrow 0$ case in question, the exchange coupling, $\hat{E}_1 \cdot \hat{E}_2$, commutes with the Zeeman interaction, $\hat{E}_{1Z} + \hat{E}_{2Z}$.

Previous descriptions of DNP have generally focused on finding the steady-state conditions reached by the various spin operators. Instead, we focus here on the time dependent evolution $O(t)$ of multiple spin states. These were calculated from the trace of their product with the state vector $\hat{\rho}(t)$ at each time step, as resulting from solving Eq. (5) by brute force using the Spinach software package. Figure 4 shows the expected time dependencies of the various electron/nuclear spin operators introduced in Equation (2), upon being disturbed from thermal equilibrium at a 14.08T field with a $\omega_{\mu w}/2\pi = 1$ MHz microwave irradiation field placed at $\pm(\omega_E + \omega_N)$. At time zero the system is equilibrated and shows negligible differences between the populations of the α and β nuclear states. The singlet and triplet electronic states populations, however, are uneven: for negative J_{ex} –which due to our negative ω_E assumption is then given by $J_{ex} = +(\omega_E + \omega_N)$ – electronic populations are ordered as $S_0 \sim T_{+1} < T_0 < T_{-1}$; for positive $J_{ex} = -(\omega_E + \omega_N)$ values, and populations vary as $T_{+1} < T_0 < T_{-1} \sim S_0$. When the microwave irradiation is turned on and an electronic saturation sets in, the populations of all electron states start to converge to similar amplitudes –but they do so at rates that depend on the α and β nuclear states: when $J_{ex} = +(\omega_E + \omega_N)$ the β state of the triplet states (Fig. 4, in blue) relaxes faster than the α state (in red), while the α state of the singlet relaxes faster than the β state of the singlet [39]. The opposite α / β behaviour arises when $J_{ex} = -(\omega_E + \omega_N)$. Still, because of the different initial conditions found when $J_{ex} = \pm(\omega_E + \omega_N)$, both situations lead to exactly the same nuclear polarization buildups. This can be appreciated by computing the time dependencies for the amplitudes of the $S_0 \hat{N}_Z$, $T_{\pm 1} \hat{N}_Z$ and $T_0 \hat{N}_Z$ operators, where such states are defined as:

$$O^{(e1e2)}\hat{N}_Z = \left| O^{(e1e2)} \right\rangle \left\langle O^{(e1e2)} \right| \hat{N}_Z = \frac{1}{2} (O_\alpha - O_\beta) \quad (8)$$

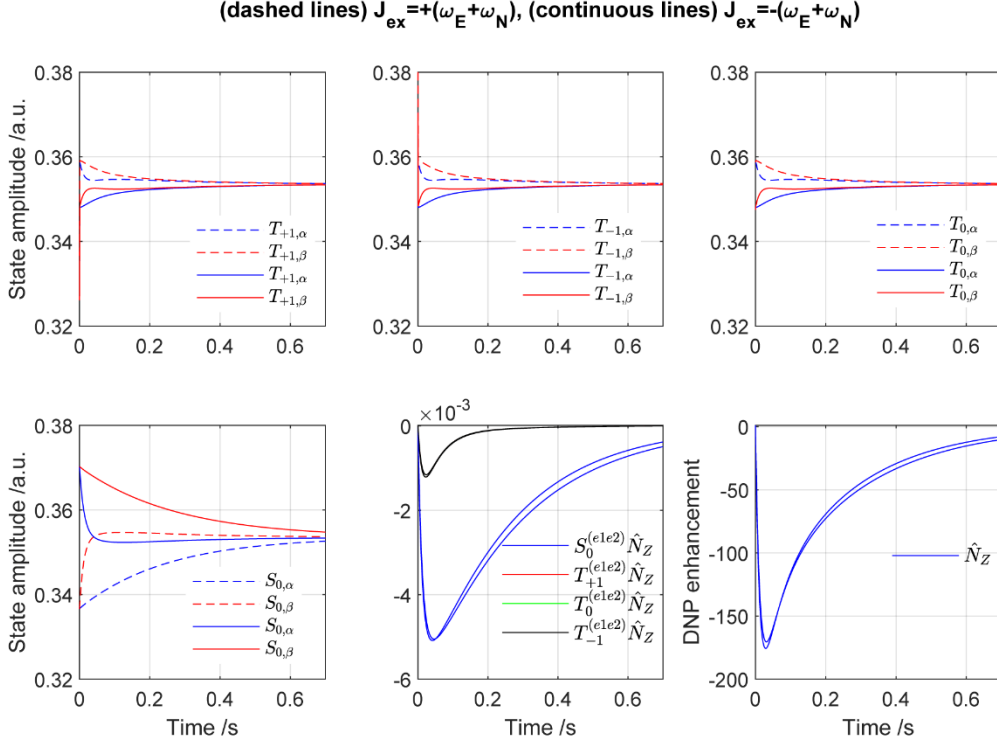


Fig. 4: Time evolution of the single-transition $S_{0,\alpha/\beta}$, $T_{\pm 1,\alpha/\beta}$ and $T_{0,\alpha/\beta}$ states; of the $\hat{N}_Z S_0$, $\hat{N}_Z T_{\pm 1}$ and $\hat{N}_Z T_0$ operators arising upon taking α and β nuclear population differences from the former; and from the overall longitudinal nuclear magnetization \hat{N}_Z ; upon subjecting a suitable biradical to DNP. All plots are normalized to a total electron spin population of one, as defined in Eqs. (S33) – (S38) in Supporting Information 3. $J_{\text{ex}} = +(\omega_E + \omega_N)$ for the dashed lines, and $J_{\text{ex}} = -(\omega_E + \omega_N)$ for the continuous lines. In the center lower plot, red and green traces are barely seen as they fall underneath an overlapping black trace. The lower right plot shows the sum of all \hat{N}_Z -related contributions, normalized by the thermal nuclear magnetization under the said conditions. For all \hat{N}_Z -containing plots, results obtained for $J_{\text{ex}} = \pm(\omega_E + \omega_N)$ are nearly overlapping. B_0 was set to 14.08 T, the rotational correlation time was set to 500 ps; all other parameters are as given in Table 1 (See Supporting Information 3 for additional definitions of the various spin operators).

where $O^{(e1e2)}$ corresponds to the electronic singlet and triplets states. $O_\alpha = S_{0,\alpha}$, $T_{\pm 1,\alpha}$ and $T_{0,\alpha}$, and $O_\beta = S_{0,\beta}$, $T_{\pm 1,\beta}$ and $T_{0,\beta}$ are then the population operators of the α and β state of the singlet and triplets, and their expressions in Cartesian operators are given in the Supporting Information 3. Notice that despite the opposite relaxation trends of the α and β nuclear states for the triplet and singlet electronic eigenstates, the amplitude of the \hat{N}_Z nuclear polarization that builds up as a result of these different relaxations ends up being sizable, independent of J_{ex} 's sign, and tracking the behaviour of the amplitude of $S_0 \hat{N}_Z$. This is because the overall nuclear magnetization given by:

$$\hat{N}_Z O_{\text{tot}} = \hat{N}_Z (S_0 + T_{+1} + T_0 + T_{-1}) = \hat{N}_Z \quad (9)$$

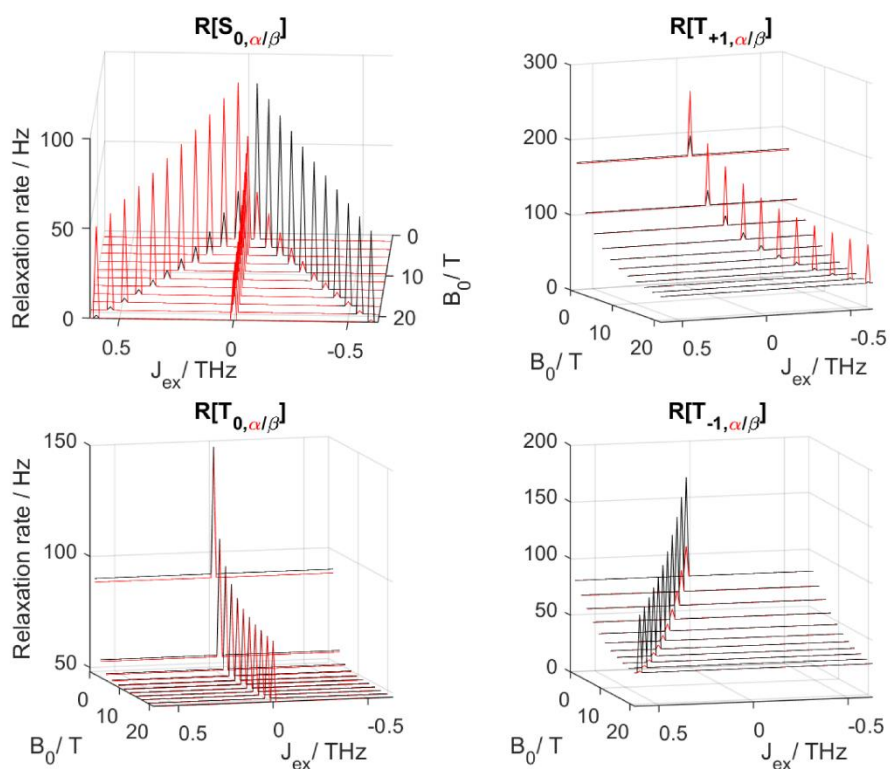
is much less influenced by the amplitudes of the $\hat{N}_Z T_{\pm 1}$ and $\hat{N}_Z T_0$ excursions, which are far smaller than those of $S_0 \hat{N}_Z$. This can be further appreciated in Supporting Information Figure S7, which shows the extent to which all these states get build up, under conditions leading to J-DNP. Notice as well that as eventually all electronic/nuclear states reach the same populations, J-DNP's build up is

transient: no nuclear polarization gains will be observed if the system is probed under steady-state conditions, of the kind usually used to explore Overhauser enhancement.

It follows that a sizable gap between the populations of the α and β nuclear states can build up, as a result of differences in the relaxation rates that electronic triplets and singlet operators associated to α and β nuclear states, will experience when $J_{\text{ex}} = \pm(\omega_E + \omega_N)$. Figure 5 presents another facet of this behaviour, by showing how the population decay rates $R[O_{\alpha/\beta}]$ of these $O_{\alpha/\beta} = T_{\pm 1, \alpha/\beta}, T_{0, \alpha/\beta}$ and $S_{0, \alpha/\beta}$ operators, change over a range of magnetic fields B_0 and exchange couplings J_{ex} . The graphs on the top of the figure depict the decay rates for these states, as calculated on the basis of brute-force numerical computations of the Redfield matrix elements. Notice that, as expected from conventional ODNP, electron-nuclear cross-relaxation rates are high and thus conducive to nuclear polarization enhancements, but only at low magnetic fields. As a result of the inverse square ω_E^{-2} dependence indicated in Eq. (1), these rates become exceedingly slow for the B_0 s of interest in normal solution-state NMR. However, marked enhancements in these rates arise whenever J_{ex} matches $\pm(\omega_E + \omega_N)$. Moreover, marked asymmetries also distinguish the relaxation rates of the α and β states associated to $T_{\pm 1, 0}$ and to S_0 . These two features are at the centre of J-DNP's nuclear enhancement: all that is needed to highlight these enhanced, asymmetric relaxation rates is to take the electronic states out of equilibrium by microwave irradiation, and capture them before they return to their final, α/β -independent, steady state saturation conditions. Supporting Information 5 provides additional characteristics about these self-relaxation rates; worth pointing out from Figures S3-S4 in that section are the differences between the rates of the α and β states in $S_0, T_{\pm 1, 0}$ with B_0 and with correlation time τ_c . Even if the absolute values of these rates decrease with both of these parameters, their differences will still lead to sizable longitudinal nuclear magnetizations, helping to understand the weak field dependence and increased efficiencies with τ_c shown for J-DNP in Figures 1-3.

The trends shown by the numerical calculations presented in Figure 5, are well reproduced by analytical expressions defining the self-relaxation rates of the various relevant populations, as they arise from Redfield's theory. These expressions were derived for the 8 eigenstates of relevance in the J-DNP process – $T_{\pm 1, \alpha/\beta}, T_{0, \alpha/\beta}$ and $S_{0, \alpha/\beta}$ – utilizing a rotating-frame approach similar to that given in [18]. These derivations, described in further detail in Supporting Information Sections 2-5, proceeded with the aid of a Mathematica-based program that performs an automated symbolic processing of the relaxation matrix. This program takes the Hamiltonian (in this case, as given in Eq. 4) and, based on the Bloch-Redfield-Wangsness theory for spin relaxation in liquids, yields the analytical expression of the coupling coefficients and the spectral density functions $J(\omega) \approx \tau_c / (1 + \tau_c^2 \omega^2)$; products of the two will in turn define the self-relaxation rates of (and cross-relaxation rate between) any (two) chosen eigenstates [21-23]. The full expressions for the self-relaxation rates R resulting from these calculations are given in Supporting Information 5, Eqs. (S44)-(S51). For the $S_{0, \alpha}$ and $S_{0, \beta}$ states, and keeping solely those terms relevant for J-DNP, these rates can be summarized as:

Numerically calculated rates



Analytically calculated rates

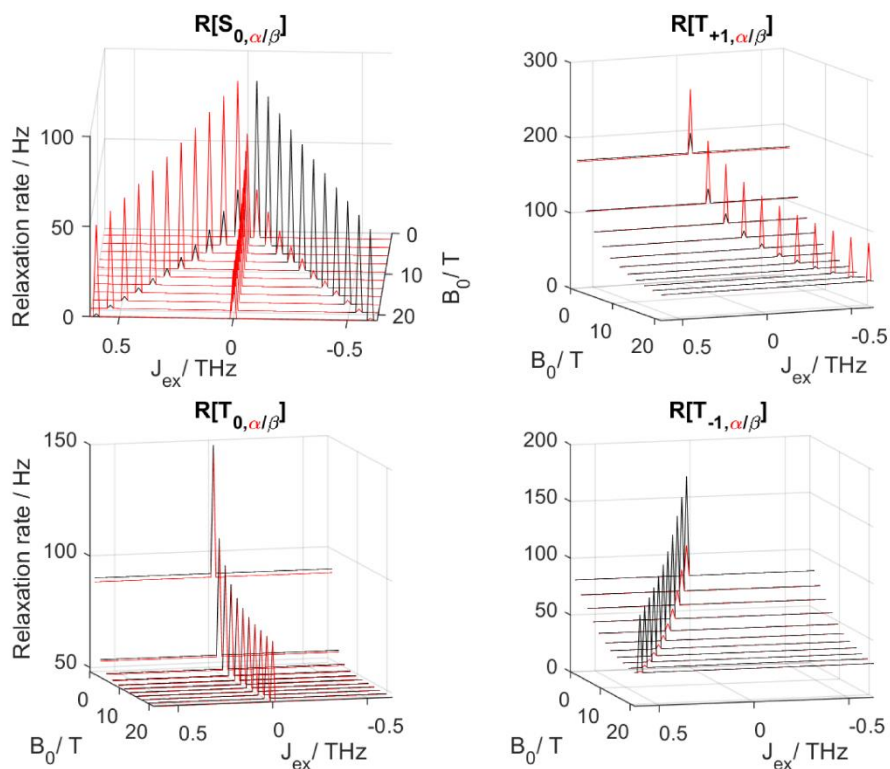


Fig. 5: Numerical (left) and analytical (right) self-relaxation rates of the singlet and the triplet electronic states associated to the α (in red) and β (in black) nuclear spin states, as a function of J_{ex} and B_0 . Calculations relied on the parameters of Table 1 and on $\tau_C = 500$ ps. Full analytical expressions for the self-relaxation rates are given in Supporting Information 5.

$$\begin{aligned}
-R[S_{0,\beta}] &= \frac{\Delta_{\Delta\text{HF}}^2}{180} J(J_{\text{ex}} - \omega_{\text{E}} + \omega_{\text{N}}) + \frac{\Delta_{\Delta\text{HF}}^2}{30} J(J_{\text{ex}} + \omega_{\text{E}} + \omega_{\text{N}}) + \\
&+ \frac{[\Delta_{\Delta\text{HF}}^2 + 4\aleph_{\Delta\text{G},\Delta\text{G}-\Delta\text{HF}}]}{120} J(J_{\text{ex}} - \omega_{\text{E}}) + \frac{[\Delta_{\Delta\text{HF}}^2 + 4\aleph_{\Delta\text{G},\Delta\text{G}-\Delta\text{HF}}]}{120} J(J_{\text{ex}} + \omega_{\text{E}}) + \dots
\end{aligned} \tag{10}$$

and

$$\begin{aligned}
-R[S_{0,\alpha}] &= \frac{\Delta_{\Delta\text{HF}}^2}{180} J(J_{\text{ex}} + \omega_{\text{E}} - \omega_{\text{N}}) + \frac{\Delta_{\Delta\text{HF}}^2}{30} J(J_{\text{ex}} - \omega_{\text{E}} - \omega_{\text{N}}) + \\
&+ \frac{[\Delta_{\Delta\text{HF}}^2 + 4\aleph_{\Delta\text{G},\Delta\text{G}+\Delta\text{HF}}]}{120} J(J_{\text{ex}} - \omega_{\text{E}}) + \frac{[\Delta_{\Delta\text{HF}}^2 + 4\aleph_{\Delta\text{G},\Delta\text{G}+\Delta\text{HF}}]}{120} J(J_{\text{ex}} + \omega_{\text{E}}) + \dots
\end{aligned} \tag{11}$$

For the $T_{+1,\alpha/\beta}$ states these were:

$$-R[T_{+1,\beta}] = \frac{\Delta_{\Delta\text{HF}}^2}{180} J(J_{\text{ex}} + \omega_{\text{E}} - \omega_{\text{N}}) + \frac{[\Delta_{\Delta\text{HF}}^2 + 4\aleph_{\Delta\text{G},\Delta\text{G}-\Delta\text{HF}}]}{120} J(J_{\text{ex}} + \omega_{\text{E}}) + \dots \tag{12}$$

and

$$-R[T_{+1,\alpha}] = \frac{\Delta_{\Delta\text{HF}}^2}{30} J(J_{\text{ex}} + \omega_{\text{E}} + \omega_{\text{N}}) + \frac{[\Delta_{\Delta\text{HF}}^2 + 4\aleph_{\Delta\text{G},\Delta\text{G}+\Delta\text{HF}}]}{120} J(J_{\text{ex}} + \omega_{\text{E}}) + \dots \tag{13}$$

For the $T_{0,\alpha/\beta}$, the self-relaxation rates are

$$-R[T_{0,\beta}] = \frac{\Delta_{\text{CSA}}^2}{15} J(\omega_{\text{N}}) + \dots \tag{14}$$

and

$$-R[T_{0,\alpha}] = \frac{\Delta_{\text{CSA}}^2}{15} J(\omega_{\text{N}}) + \dots \tag{15}$$

And for $T_{-1,\alpha/\beta}$ the self-relaxation rates were:

$$-R[T_{-1,\beta}] = \frac{\Delta_{\Delta\text{HF}}^2}{30} J(J_{\text{ex}} - \omega_{\text{E}} - \omega_{\text{N}}) + \frac{[\Delta_{\Delta\text{HF}}^2 + 4\aleph_{\Delta\text{G},\Delta\text{G}-\Delta\text{HF}}]}{120} J(J_{\text{ex}} - \omega_{\text{E}}) + \dots \tag{16}$$

and

$$-R[T_{-1,\alpha}] = \frac{\Delta_{\Delta\text{HF}}^2}{180} J(J_{\text{ex}} - \omega_{\text{E}} + \omega_{\text{N}}) + \frac{[\Delta_{\Delta\text{HF}}^2 + 4\aleph_{\Delta\text{G},\Delta\text{G}+\Delta\text{HF}}]}{120} J(J_{\text{ex}} - \omega_{\text{E}}) + \dots \tag{17}$$

Here, $\Delta\mathbf{G} = \mathbf{G}_1 - \mathbf{G}_2$ and $\Delta\mathbf{HF} = \mathbf{HFC}_1 - \mathbf{HFC}_2$ are anisotropies deriving from tensors associated to the differences between the two g- and electron/nuclear hyperfine coupling tensors, respectively; \mathbf{CSA} is the chemical shift anisotropy tensor; and as is usual in spin relaxation theory [21, 22, Supporting Information 4], all these rates contain combinations of second-rank norms squared $\Delta_{\mathbf{A}}^2$ of all the aforementioned tensors \mathbf{A} [40]. As mentioned, for normal liquids $J(\omega) \approx 0$ for all cases other than when involving frequencies $\omega/2\pi \leq 1$ GHz. This means that for the B_0 fields used in conventional NMR all contributions to the rates in Eqs. (8)-(15) can be disregarded, whenever including an ω -argument term that either isn't $J(\omega_{\text{N}})$, or is not made zero by J_{ex} . The latter are the potentially important terms that were kept in these equations, and they include a variety of $J_{\text{ex}} = \pm\omega_{\text{E}}$ conditions; inspection of these terms, however, shows that they will not always conduce to the build-up of nuclear polarization. Indeed, whenever these $J(J_{\text{ex}} \pm \omega_{\text{E}} \pm \omega_{\text{N}})$ terms modulate g-anisotropies, they contribute by exactly the same measures to the relaxation rate of their associated O_{α} and O_{β} electron spin states. The same happens for all $J(\omega_{\text{N}})$ -containing terms. No differentials in nuclear polarizations will therefore be built by any of these. By contrast, in the presence of a substantial difference in the hyperfine couplings

between either electron and the nuclear spin, large differences can arise between the self-relaxation rates of certain O_α and O_β spin states. This can be most easily appreciated for $S_{0,\alpha}$ and $S_{0,\beta}$ relaxation rates: the latter will be dominated by the $J(J_{\text{ex}} + \omega_E + \omega_N)$ term if $J_{\text{ex}} = -(\omega_E + \omega_N)$, and the former by the $J(J_{\text{ex}} - \omega_E - \omega_N)$ if $J_{\text{ex}} = +(\omega_E + \omega_N)$. Either case, such J_{ex} conditions will result in marked differences between $R[S_{0,\alpha}]$ and $R[S_{0,\beta}]$; The situation is less marked in the case of the $R[T_{\pm 1,\alpha/\beta}]$ self-relaxation rates: In the $J_{\text{ex}} = \pm(\omega_E + \omega_N)$ case there will also be differences between them and such states can thus also be conducive to nuclear build ups, even if their influence will in general be smaller than that imparted by the single. Finally, the self-relaxation rates $R[T_{0,\beta}]$ and $R[T_{0,\alpha}]$ do not contain spectral densities of the form $J(J_{\text{ex}} \pm \omega_E + \omega_N)$ that could lead to significant populations imbalances between the α and β states. All these features are summarized in the lower four panels of Figure 5, which show the rates expected from Eqs. (8)-(15) for a biradical with the parameters in Table 1. Notice the agreement between these analytical rate predictions, and the aforementioned numerical results presented on the top panels of Figure 5.

4. Conclusions and outlook

The present study discussed a proposal for enhancing signals in solution state NMR, that could provide substantial sensitivity gains for a wide range of B_0 magnetic fields, and τ_c rotational correlation times. Like the CCDNP proposal, this new J-DNP mechanism is based on biradicals; yet the conditions that J-DNP exploits are transient, emerging at what to our knowledge is the hitherto unexplored $J_{\text{ex}} \approx \pm(\omega_E + \omega_N)$ regime. Both brute-force numerical simulations based on the Liouville-van Neumann equation and analytical derivations based on the relaxation rates predicted by Redfield theory, provided coinciding predictions regarding the realization of significant NMR polarization buildups. These nuclear enhancements required irradiation times lasting a fraction of a second, but if implemented at the right frequency they should not require inordinately strong microwave fields, and appear to operate over a range of 0.1-1 ns correlation times. The weak dependence on microwave power that these calculations evidenced for the nuclear enhancement reflect the easiness with which, for the conditions of Table 1 (further analysed in Supporting Information 1), the electronic spin states could be taken out of equilibrium. It remains to be seen if practical setups enable the experimental realization of such conditions. Table 1 assumed that the two electrons had identical g-tensors, with electronic and nuclear Zeeman couplings made anisotropic for the sake of realism. Supporting Information 6 demonstrates that very similar kinds of enhancements are reached if either the radicals or the nucleus have zero g- and shielding anisotropies –as these are not really requirements of the method. In this case the enhancement will also arise if the isotropic g-values of the two electrons differ (Supporting Fig. S10); however, the requirement for identical g-anisotropies is critical: if the two electrons have different anisotropic g-tensors, these will overtake at high fields the subtle differential nuclear spin relaxation mechanisms arising from the different hyperfine couplings, effectively “killing” the enhancement (Supporting Figure S11). Also, as in CIDNP’s radical pair mechanism demanding differences between the electrons’ coupling to the α and β nuclear spin states [27, 28], J-DNP also requires differential hyperfine couplings driving a differential relaxation-based “nuclear spin-state filtration” by singlet and triplet electronic states; in their absence, for instance if the nucleus is symmetrically placed between the two electrons (Supporting Figure S12), no enhancement results.

Likewise, the enhancement will tend to zero if the nucleus remains too distant from the biradical (Fig. 6): for instance, a proton placed 20 Å away from the biradical may require over 1 s to achieve significant polarization gains – a time by which the DNP effect will lose against competing pathways. Interestingly, despite that J-DNP follows from effects originating in second-rank spherical anisotropies, its nuclear enhancement never changes sign (Figure 6). This is important, as otherwise the spatial averaging brought about by molecular translations, could end up being smaller or even zero.

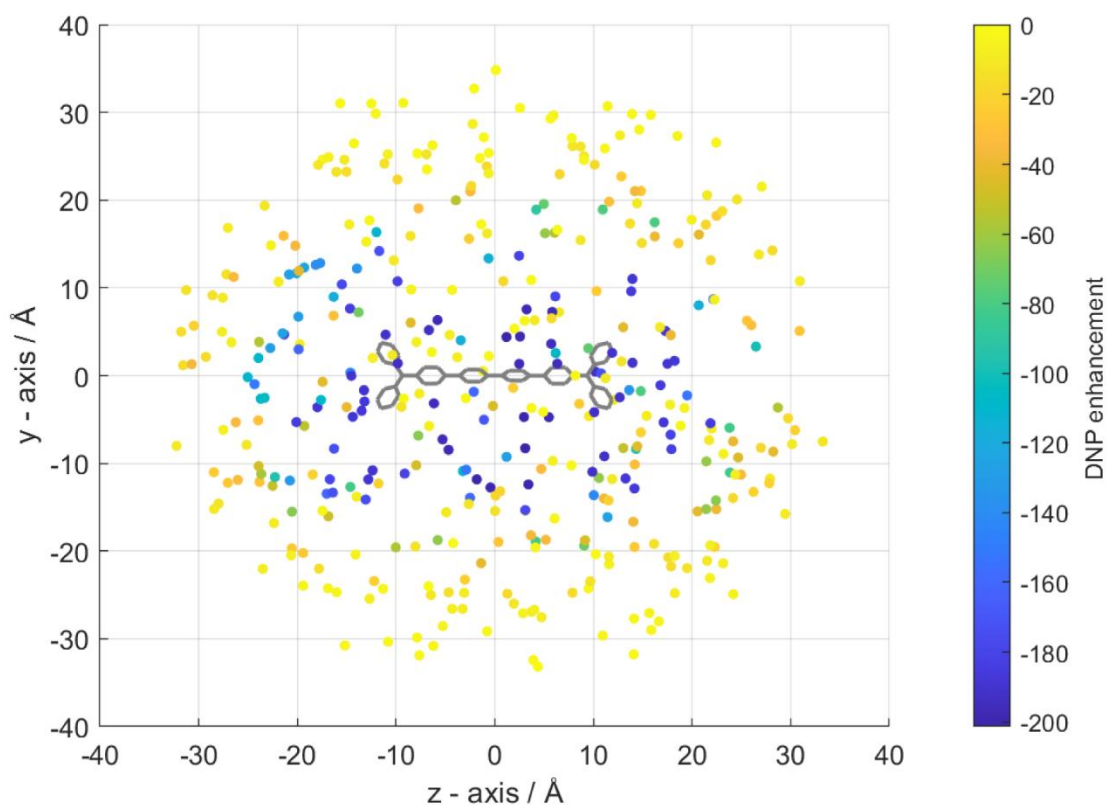


Fig. 6: Maximum enhancement (amplitude of \hat{N}_z normalized to the thermal equilibrium value) achieved within 500 ms of J-DNP enhancement, as a function of random ^1H -coordinates surrounding a model biradical (grey structure in the centre). Parameters included $B_0 = 14.08 \text{ T}$, $\tau_c = 500 \text{ ps}$, other conditions as given in Table 1. Notice the negative enhancement displayed by all positions surrounding the radical, leading to an ensemble averaging that will be different from zero regardless of nuclear displacements vs the biradical's center.

Despite leading to overall encouraging features, the present study also invoked a number of strong assumptions. These included the absence of isotropic hyperfine interactions to any nucleus, something which for certain trityl biradicals might call for perdeuteration. It was also assumed that the non-Redfield relaxation terms in monoradicals resembled those acting in biradicals (Supporting Information 1); it remains to be seen how realistic this assumption was. Last but not least, a major approximation taken in this study was assuming a fixed electron/electron/nuclear geometry over the course of the DNP process: as the latter requires 10-100 ms and molecules in regular liquids diffuse tens of microns over such times, this fixed molecular geometry assumption is clearly unrealistic. On the other hand, a similar fixed-geometry assumption is successfully used and leads to realistic predictions in conventional ODNP, where it works by virtue of ODNP's independence on maintaining

specific correlations. Likewise, we hypothesize that the different $R[O_{\alpha/\beta}]$ rates required for supporting J-DNP, will be preserved regardless of the transient contact that a specific nucleus makes with an ensemble of biradicals over the course of its spin polarization process. This turns out as another potential advantage over the CCDNP proposal, which required the three-spin correlations to be kept until the steady-state enhancement was reached. Experiments are in course, to evaluate the correctness of such assumptions.

5. Acknowledgments

This project was funded by the Weizmann-UK Joint Research Programme, the Israel Science Foundation (ISF 965/18), the Perlman Family Foundation, and the US National Science Foundation (grants numbers CHE-1808660, DMR-1644779). MGC acknowledges Weizmann's Faculty of Chemistry for a Dean Fellowship. LF holds the Bertha and Isadore Gudelsky Professorial Chair and Heads the Clore Institute for High-Field Magnetic Resonance Imaging and Spectroscopy, whose support is acknowledged.

6. Author contribution

LF and MGC discovered the J-DNP effect and provided a theoretical description of its mechanism. MGC and IK provided tools for its corroboration. MG conducted the spin dynamics simulations and derived the equations. All authors discussed and wrote the paper.

7. Competing interests

The authors declare no competing interests.

8. References

1. Overhauser, A.W., *Polarization of nuclei in metals*. Physical Review, 1953. **92**(2): p. 411.
2. Carver, T.R. and C.P. Slichter, *Experimental verification of the Overhauser nuclear polarization effect*. Physical Review, 1956. **102**(4): p. 975.
3. Hu, K.-N., et al., *Dynamic nuclear polarization with biradicals*. Journal of the American Chemical Society, 2004. **126**(35): p. 10844.
4. Bajaj, V.S., et al., *250 GHz CW gyrotron oscillator for dynamic nuclear polarization in biological solid state NMR*. Journal of Magnetic Resonance, 2007. **189**(2): p. 251.
5. Bajaj, V., et al., *Dynamic nuclear polarization at 9 T using a novel 250 GHz gyrotron microwave source*. Journal of Magnetic Resonance, 2011. **213**(2): p. 404.
6. Hu, K.N., et al., *Quantum mechanical theory of dynamic nuclear polarization in solid dielectrics*. The Journal of Chemical Physics, 2011. **134**(12): p. 125105.
7. Ardenkjaer-Larsen, J.H., et al., *Increase in signal-to-noise ratio of > 10,000 times in liquid-state NMR*. Proceedings of the National Academy of Sciences of the USA, 2003. **100**(18): p. 10158.
8. Golman, K., et al., *Metabolic imaging by hyperpolarized ^{13}C magnetic resonance imaging for in vivo tumor diagnosis*. Cancer research, 2006. **66**(22): p. 10855.
9. Dubroca, T., et al., *Large volume liquid state scalar Overhauser dynamic nuclear polarization at high magnetic field*. Physical Chemistry Chemical Physics, 2019. **21**(38): p. 21200.
10. Parigi, G., et al., *Understanding Overhauser Dynamic Nuclear Polarisation through NMR relaxometry*. Molecular Physics, 2019. **117**(7-8): p. 888.
11. Levien, M., et al., *Nitroxide Derivatives for Dynamic Nuclear Polarization in Liquids: The Role of Rotational Diffusion*. The Journal of Physical Chemistry Letters, 2020. **11**(5): p. 1629.

12. Loening, N.M., et al., *Solution-state dynamic nuclear polarization at high magnetic field*. Journal of the American Chemical Society, 2002. **124**(30): p. 8808.
13. Liu, G.Q., et al., *One-thousand-fold enhancement of high field liquid nuclear magnetic resonance signals at room temperature*. Nature Chemistry, 2017. **9**(7): p. 676-680.
14. Hausser, K.H. and D. Stehlik, *Dynamic nuclear polarization in liquids*, in *Advances in Magnetic and Optical Resonance*. 1968, Elsevier. p. 79.
15. Griesinger, C., et al., *Dynamic nuclear polarization at high magnetic fields in liquids*. Progress in Nuclear Magnetic Resonance Spectroscopy, 2012. **64**: p. 4.
16. Prisner, T., V. Denysenkov, and D. Sezer, *Liquid state DNP at high magnetic fields: Instrumentation, experimental results and atomistic modelling by molecular dynamics simulations*. Journal of Magnetic Resonance, 2016. **264**: p. 68.
17. Ravera, E., C. Luchinat, and G. Parigi, *Basic facts and perspectives of Overhauser DNP NMR*. Journal of Magnetic Resonance, 2016. **264**: p. 78.
18. Concilio, M.G., et al., *High-field solution state DNP using cross-correlations*. Journal of Magnetic Resonance, 2021. **326**: p. 106940.
19. Reginsson, G.W., et al., *Trityl radicals: spin labels for nanometer-distance measurements*. Chemistry, 2012. **18**(43): p. 13580.
20. Jassoy, J.J., et al., *Synthesis of Nanometer Sized Bis- and Tris-trityl Model Compounds with Different Extent of Spin-Spin Coupling*. Molecules, 2018. **23**(3): p. 682.
21. Redfield, A., *The theory of relaxation processes*, in *Advances in Magnetic and Optical Resonance*. 1965, Elsevier. p. 1.
22. Goldman, M., *Formal theory of spin--lattice relaxation*. J Magn Reson, 2001. **149**(2): p. 160.
23. Kuprov, I., N. Wagner-Rundell, and P. Hore, *Bloch-Redfield-Wangsness theory engine implementation using symbolic processing software*. Journal of Magnetic Resonance, 2007. **184**(2): p. 196.
24. Kuprov, I., *Diagonalization-free implementation of spin relaxation theory for large spin systems*. Journal of Magnetic Resonance, 2011. **209**(1): p. 31.
25. Goodwin, D. and I. Kuprov, *Auxiliary matrix formalism for interaction representation transformations, optimal control, and spin relaxation theories*. The Journal of chemical physics, 2015. **143**(8): p. 084113.
26. Bargon, J., H. Fischer, and U. Johnsen, *Kernresonanz-Emissionslinien während rascher Radikalreaktionen*. Zeitschrift für Naturforschung A, 1967. **22**: p. 1551.
27. Kaptein, R. and L.J. Oosterhoff, *Chemically induced dynamic nuclear polarization II: (Relation with anomalous ESR spectra)*. Chem. Phys. Lett., 1969. **4**(4): p. 195.
28. Closs, G.L., *Mechanism explaining nuclear spin polarizations in radical combination reactions*. J. Am. Chem. Soc. , 1971. **93**(6): p. 1546.
29. Santabarbara, S., et al., *Bidirectional electron transfer in photosystem I: determination of two distances between P700+ and A1- in spin-correlated radical pairs*. Biochemistry, 2005. **44**(6): p. 2119.
30. Yong, L., et al., *Electron spin relaxation of triarylmethyl radicals in fluid solution*. J Magn Reson, 2001. **152**(1): p. 156.
31. Owenius, R., G.R. Eaton, and S.S. Eaton, *Frequency (250 MHz to 9.2 GHz) and viscosity dependence of electron spin relaxation of triarylmethyl radicals at room temperature*. Journal of Magnetic Resonance, 2005. **172**(1): p. 168.
32. Kuprov, I., et al., *Anomalous Nuclear Overhauser Effects in Carbon-Substituted Aziridines: Scalar Cross-Relaxation of the First Kind*. Angewandte Chemie International Edition, 2015. **54**(12): p. 3697.
33. Hogben, H., et al., *Spinach - a software library for simulation of spin dynamics in large spin systems*. Journal of Magnetic Resonance, 2011. **208**(2): p. 179.
34. Ardenkjaer-Larsen, J.H., et al., *EPR and DNP properties of certain novel single electron contrast agents intended for oximetric imaging*. Journal of Magnetic Resonance, 1998. **133**(1): p. 1.

35. Hore, P.J. and R.W. Broadhurst, *Photo-CIDNP of biopolymers*. Prog. NMR Spectrosc., 1993. **25**(4): p. 345.
36. Vega, S., *Fictitious spin 1/2 operator formalism for multiple quantum NMR*. J. Chem. Phys., 1978. **68**: p. 5518.
37. Wangsness, R.K. and F. Bloch, *The dynamical theory of nuclear induction*. Physical Review, 1953. **89**(4): p. 728.
38. Levitt, M.H. and L. Di Bari, *Steady state in magnetic resonance pulse experiments*. Phys Rev Lett, 1992. **69**(21): p. 3124-3127.
39. Kuprov, I., et al., *Spin relaxation effects in photochemically induced dynamic nuclear polarization spectroscopy of nuclei with strongly anisotropic hyperfine couplings*. Journal of the American Chemical Society, 2007. **129**(29): p. 9004-9013.
40. Blicharski, J., *Nuclear magnetic relaxation by anisotropy of the chemical shift*. Z Naturforsch Pt A, 1972. **27**: p. 1456.

Supplementary Information for

J-driven Dynamic Nuclear Polarization: A new mechanism for sensitizing high field solution state NMR

Maria Grazia Concilio^{1*}, Ilya Kuprov², Lucio Frydman,^{1,3*}

¹Department of Chemical and Biological Physics, Weizmann Institute of Science, Rehovot, Israel.

²School of Chemistry, University of Southampton, Southampton, UK.

³National High Magnetic Field Laboratory, Tallahassee, Florida, USA.

Supporting Information 1: R_1/R_2 relaxation rate analyses for mono- and bis-trityl radicals

As this is a purely theoretical study, we consider it necessary to test our numerical simulations against some set of experimental parameters. Given the paucity of solution-state NMR data about biradicals' relaxation rates, the theoretical models were used to estimate the electronic longitudinal and transverse relaxation rates for trityl monoradicals –for which solution-state measurements have been reported in Refs. [1, 2]. Following the treatment given in Ref. [1], the electronic R_1 rate for this radical will be assumed given by three contributions

$$\begin{aligned} R_{1,\text{total}} &= R_{1,\text{local}} + R_{1,\text{BRW}} + R_{1,\text{solvent}} \\ &\approx R_{1,\text{local}} + R_{1,\text{BRW}} \end{aligned} \quad (\text{S1a})$$

Here $R_{1,\text{local}}$ is the self-relaxation rate arising from the local vibrational modes related to the stretching of bonds in the radical, and is a magnetic field independent contribution estimated by Eaton et al [1] as 5.9×10^4 Hz for per-deutero and 6.1×10^4 Hz for per-protio trityls.

$$R_{1,\text{BRW}} = n \left[\underbrace{\left(\frac{\Delta_{\text{HF, intra}}^2}{9} \right) \left(\frac{\tau_{\text{C}}}{(1 + \tau_{\text{C}}^2 \omega_{\text{E}}^2)} \right)}_{\text{hyperfine relaxation}} \right] + \underbrace{\left(\frac{2\Delta_{\text{G}}^2}{15} \right) \left(\frac{\tau_{\text{C}}}{(1 + \tau_{\text{C}}^2 \omega_{\text{E}}^2)} \right)}_{\text{g-anisotropy relaxation}} \quad (\text{S1b})$$

is the relaxation rate which arises from the stochastic modulation of the radical's g -tensor anisotropy and of the hyperfine interactions between the electron and the n protons interacting with it within the radical; this is the kind of rates computed in the main text based on Bloch-Redfield-Wangsness theory in terms of Δ_{G}^2 and $\Delta_{\text{HF, intra}}^2$ coupling strengths; i.e., of the second-rank norm squared defined in Supporting Information 4, for the g -anisotropy and the hyperfine interaction tensors. Finally,

$$R_{1,\text{solvent}} = n_{\text{solv}} \left[\left(\frac{\Delta_{\text{HF, inter}}^2}{9} \right) \left(\frac{\tau_{\text{solv}}}{(1 + \tau_{\text{solv}}^2 \omega_{\text{E}}^2)} \right) \right] \quad (\text{S1c})$$

is an *ad hoc* relaxation term, arising from the dipolar interaction between the electron and n_{solv} solvent molecules; the coupling strength of this relaxation is given by the second-rank norm squared of the dipolar interaction tensor between the electron and the solvent protons $\Delta_{\text{HF,inter}}^2$, and by a correlation time τ_{solvent} . Eaton et al in Ref. [1] have estimated the $R_{1,\text{solvent}}$ in Eq. (S1c) as $\tau_{\text{solvent}} = F \tau_C$, where F is a ratio between the solvent correlation time and the trityl correlation time, that is different for each radical. As this latter term is much smaller than the remaining relaxation rates it is henceforth ignored in both the mono- and bi-radical estimations. Finally, in a non-viscous solvent, the $R_{2,\text{total}}$ corresponds to $R_{1,\text{total}} + R_{2,\text{BRW}}$ [1]. The BRW theory predicts this second term to be

$$R_{2,\text{BRW}} = n \left[\underbrace{\left(\frac{\Delta_{\text{HF,trityl}}^2}{90} \right) \left(2 + \frac{5\tau_C}{(1 + \tau_C^2 \omega_E^2)} + \frac{3\tau_C}{(1 + \tau_C^2 \omega_N^2)} \right)}_{\text{hyperfine relaxation}} \right] + \underbrace{\left(\frac{\Delta_G^2}{45} \right) \left(4 + \frac{3\tau_C}{(1 + \tau_C^2 \omega_E^2)} \right)}_{\text{g-anisotropy relaxation}} \quad (\text{S2})$$

Table S1 compares the $R_{1,\text{total}}$ and $R_{2,\text{total}}$ values determined from Eqs. (S1) and (S2), with values reported experimentally in Ref. [1] for per-protio and per-deutero trityls at different fields. There is good agreement between both sets. Notice, however, that the low magnetic fields explored in this comparison, it is the local vibrational modes contributing to $R_{1,\text{local}}$ that dominate the longitudinal- and transverse relaxation rates. As this parameter was estimated from the experimental data, the good agreement is not surprising.

Table S1: Comparison between T_1 and T_2 calculated using Eq. (S1) and Eq. (S2) and experimental T_1 and T_2 in water for trityl- CD_3 and trityl- CH_3 obtained from [1]. n represents the number of trityl protons dipole-coupled to the radical. For trityl- CH_3 , the distances between the electron and all 36 protons in the radical were set equal to 5.3 Å.

Magnetic field / T	R_1 from Eq. 1 / Hz	Experimental R_1 / Hz	R_2 from Eq. 2 / Hz	Experimental R_2 / Hz
Trityl-CD_3 radical, $n = 0$, $R_{1,\text{local}} = 0.59 \times 10^5$ Hz				
0.33 T (X-band)	5.9×10^4	5.9×10^4	6.7×10^4	9.1×10^4
0.11 T (S-band)	5.9×10^4	6.2×10^4	6.2×10^4	8.3×10^4
0.03 T (L-band)	5.9×10^4	7.2×10^4	6.2×10^4	8.3×10^4
9×10^{-3} T (250 MHz)	6.2×10^4	/	6.2×10^4	9.1×10^4
Trityl-CH_3 radical $\rightarrow n = 36$, $R_{1,\text{local}} = 0.61 \times 10^5$ Hz				
0.33 T (X-band)	6.2×10^4	6.2×10^4	2.3×10^5	1.1×10^5
0.11 T (S-band)	6.6×10^4	7.1×10^4	1.0×10^5	1.1×10^5
0.03 T (L-band)	8.3×10^4	8.3×10^4	1.1×10^5	1.1×10^5
9×10^{-3} T (250 MHz)	9.1×10^4	/	1.3×10^5	1.3×10^5

It is enlightening to extend this monoradical analysis to the case of trityl bi-radicals. In this case it is reasonable to assume that the contributions coming from solvent-induced and bond-vibration-induced terms to R_1 relaxation, will remain similar as those given in Table S1. The electronic $R_{1,\text{BRW}}$ and

$R_{2, \text{BRW}}$ longitudinal and transverse rates, however, will be significantly increased by the electron-electron dipolar interaction, and will now be dominated by $J(0)$ -containing terms that depend on the rotational correlation time but are independent from the magnetic field. A full analysis of these two terms leads to

$$\begin{aligned}
R_{1, \text{BRW}} = -R[\hat{E}_Z] &= \frac{\Delta_{\text{EE}}^2}{90} J(0) + \frac{\mathfrak{N}_{(\text{HFC}, \Sigma\text{HF}), \text{inter}}}{18} J(\omega_{\text{E}}) + \\
&+ \frac{\mathfrak{N}_{(\text{HFC}, \Delta\text{HF}), \text{inter}}}{360} \left[3J(J_{\text{ex}} + \omega_{\text{E}}) + 3J(J_{\text{ex}} - \omega_{\text{E}}) + 6J(J_{\text{ex}} + \omega_{\text{E}} + \omega_{\text{N}}) + \right. \\
&\quad \left. + 6J(J_{\text{ex}} - \omega_{\text{E}} - \omega_{\text{N}}) + J(J_{\text{ex}} + \omega_{\text{E}} - \omega_{\text{N}}) + J(J_{\text{ex}} - \omega_{\text{E}} + \omega_{\text{N}}) \right] + \\
&+ \mathfrak{n} \left(\frac{\mathfrak{N}_{(\text{HFC}, \Sigma\text{HF}), \text{intra}}}{18} J(\omega_{\text{E}}) + \right. \\
&\quad \left. \frac{\mathfrak{N}_{(\text{HFC}, \Delta\text{HF}), \text{intra}}}{360} \left[3J(J_{\text{ex}} + \omega_{\text{E}}) + 3J(J_{\text{ex}} - \omega_{\text{E}}) + 6J(J_{\text{ex}} + \omega_{\text{E}} + \omega_{\text{N}}) + \right. \right. \\
&\quad \left. \left. + 6J(J_{\text{ex}} - \omega_{\text{E}} - \omega_{\text{N}}) + J(J_{\text{ex}} + \omega_{\text{E}} - \omega_{\text{N}}) + J(J_{\text{ex}} - \omega_{\text{E}} + \omega_{\text{N}}) \right] \right) + \\
&+ \frac{[4\mathfrak{N}_{\text{G}, \Delta\text{G}} + 2\mathfrak{N}_{\text{EE}, -\Delta\text{G}}]}{120} J(J_{\text{ex}} - \omega_{\text{E}}) + \frac{[4\mathfrak{N}_{\text{G}, \Delta\text{G}} + 2\mathfrak{N}_{\text{EE}, \Delta\text{G}}]}{120} J(J_{\text{ex}} + \omega_{\text{E}}) + \\
&+ \frac{[3\Delta_{\text{EE}}^2 + 6\mathfrak{N}_{\text{G}, \Sigma\text{G}}]}{90} J(\omega_{\text{E}}) + \frac{\Delta_{\text{EE}}^2}{15} J(2\omega_{\text{E}})
\end{aligned} \tag{S3}$$

and

$$\begin{aligned}
R_{2, \text{BRW}} = -R[\hat{E}_+] &= \frac{\Delta_{\text{EE}}^2}{36} J(0) + \frac{4\mathfrak{N}_{\text{G}, \Sigma\text{G}}}{90} J(0) + \\
&+ \frac{\mathfrak{N}_{(\text{HFC}, \Sigma\text{HF}), \text{inter}}}{90} J(0) + \frac{\mathfrak{N}_{(\text{HFC}, \Sigma\text{HF}), \text{inter}}}{120} J(\omega_{\text{N}}) + \frac{\mathfrak{N}_{(\text{HFC}, \Sigma\text{HF}), \text{inter}}}{36} J(\omega_{\text{E}}) + \\
&+ \frac{\mathfrak{N}_{(\text{HFC}, \Delta\text{HF}), \text{inter}}}{720} \left[3J(J_{\text{ex}} - \omega_{\text{E}}) + 3J(J_{\text{ex}} + \omega_{\text{E}}) + 12J(J_{\text{ex}} - \omega_{\text{E}} - \omega_{\text{N}}) + 12J(J_{\text{ex}} + \omega_{\text{E}} - \omega_{\text{N}}) + \right. \\
&\quad \left. + J(J_{\text{ex}} - \omega_{\text{E}} + \omega_{\text{N}}) + 6J(J_{\text{ex}} + \omega_{\text{N}}) + 6J(J_{\text{ex}} + \omega_{\text{E}} + \omega_{\text{N}}) \right] + \\
&+ \mathfrak{n} \left(\frac{\mathfrak{N}_{(\text{HFC}, \Sigma\text{HF}), \text{intra}}}{90} J(0) + \frac{\mathfrak{N}_{(\text{HFC}, \Sigma\text{HF}), \text{intra}}}{120} J(\omega_{\text{N}}) + \frac{\mathfrak{N}_{(\text{HFC}, \Sigma\text{HF}), \text{intra}}}{36} J(\omega_{\text{E}}) + \right. \\
&\quad \left. \frac{\mathfrak{N}_{(\text{HFC}, \Delta\text{HF}), \text{intra}}}{720} \left[3J(J_{\text{ex}} - \omega_{\text{E}}) + 3J(J_{\text{ex}} + \omega_{\text{E}}) + 12J(J_{\text{ex}} - \omega_{\text{E}} - \omega_{\text{N}}) + 12J(J_{\text{ex}} + \omega_{\text{E}} - \omega_{\text{N}}) + \right. \right. \\
&\quad \left. \left. + J(J_{\text{ex}} - \omega_{\text{E}} + \omega_{\text{N}}) + 6J(J_{\text{ex}} + \omega_{\text{N}}) + 6J(J_{\text{ex}} + \omega_{\text{E}} + \omega_{\text{N}}) \right] \right) + \\
&+ \frac{[4\mathfrak{N}_{\text{G}, \Delta\text{G}} + 2\mathfrak{N}_{\text{EE}, \Delta\text{G}}]}{240} J(J_{\text{ex}} - \omega_{\text{E}}) + \frac{[4\mathfrak{N}_{\text{G}, \Delta\text{G}} + 2\mathfrak{N}_{\text{EE}, -\Delta\text{G}}]}{240} J(J_{\text{ex}} + \omega_{\text{E}}) + \\
&+ \frac{[9\Delta_{\text{EE}}^2 + 6\mathfrak{N}_{\text{G}, \Sigma\text{G}}]}{180} J(\omega_{\text{E}}) + \frac{\Delta_{\text{EE}}^2}{30} J(2\omega_{\text{E}})
\end{aligned} \tag{S4}$$

where the symbols are as described in the Supplementary Information 4, and we have made a distinction between hyperfine couplings with n protons within the biradical (“intra”), and with one proton that belongs to the solvent and could be a target of ODNP (“inter”). At the fields of interest in our studies, all spectral densities that have the electron and the nuclear Larmor frequency in them can be disregarded. This leaves solely the terms involving zero-frequency spectral densities

$$R_{1, \text{BRW}} = -R[\hat{E}_Z] \simeq \frac{\Delta_{\text{EE}}^2}{90} J(0) \tag{S5}$$

and

$$R_{2,\text{BRW}} = -R[\hat{E}_+] = \frac{\Delta_{\text{EE}}^2}{36} J(0) + \frac{4\aleph_{\text{G},\Sigma\text{G}}}{90} J(0) + \frac{\aleph_{(\text{HFC},\Sigma\text{HF}),\text{inter}}}{90} J(0) + n \left(\frac{\aleph_{(\text{HFC},\Sigma\text{HF}),\text{intra}}}{90} J(0) \right) \quad (\text{S6})$$

$R_{1,\text{BRW}}$ is thus dominated by Δ_{EE}^2 , i.e., by the dipolar interaction between electrons; and $R_{2,\text{BRW}}$ is dominated by this term as well as by the second rank scalar products $\aleph_{\text{G},\Sigma\text{G}}$ and $\aleph_{\text{HFC},\Sigma\text{HF}}$ between the g-tensor of one electron and the sum of the two g-tensors, and by the hyperfine coupling between one electron and one proton, and the sum of the hyperfines of the two electrons and one proton, respectively. The magnitudes of the coefficients in Eq. (S3) and Eq. (S4) for the case of a bis-trityl-type biradical, are shown in the Table S1. These coefficients will scale according to spectral densities; Figure S1 show how these BRW-derived R_1 and R_2 terms change with the biradical's correlation time τ_c . These rates should be compared with the relaxivity contributions arising from the vibrational local modes, which are likely to be in the order of what they were for the monotrityl radical –i.e., $\approx 5 \cdot 10^4$ Hz. It follows that for the trityl bis-radical the contribution of these $R_{1,\text{local}}$ will no longer be dominant, primarily due to the onset of relaxation effects driven by Δ_{EE}^2 and $\aleph_{\text{G},\Sigma\text{G}}$ (the latter mostly at the high fields of interest; Table 1).

Table S2: Magnitude of the second-rank norm squared and the scalar products (defined in Supporting Information 4) predicted by Eqs. (S5) and (S6), for a trityl-based biradical with parameters as given in the Table 1.

$\Delta_{\text{A}}^2 / \aleph_{\text{A,B}}$	Magnitude / (rad/s) ²
Δ_{EE}^2	2×10^{16}
$\aleph_{\text{G},\Delta\text{G}}$	472
$\aleph_{\text{G},\Sigma\text{G}}$	2×10^{17}
$\aleph_{\text{EE},\Delta\text{G}} (\aleph_{\text{EE},-\Delta\text{G}})$	687699 / -687699
$\aleph_{(\text{HFC},\Sigma\text{HF}),\text{intra}} / \aleph_{(\text{HFC},\Sigma\text{HF}),\text{inter}}^1$	$1.30 \times 10^{13} / 4.9 \times 10^{13}$
$\aleph_{(\text{HFC},\Delta\text{HF}),\text{intra}} / \aleph_{(\text{HFC},\Delta\text{HF}),\text{inter}}^1$	$1.34 \times 10^{13} / 5.1 \times 10^{13}$

¹ The intra-molecular dipolar interaction between the electron and the methyl protons in each trityl group of the biradical was computed setting a proton-electron distance equal to 5.3 Å (between the proton and its closest electron; electron/proton hyperfine couplings between the two trityls in the molecule were disregarded). The inter-molecular dipolar interaction between the electron and the solvent was computed setting a proton-electron distance equal to 8.3 Å (again: between the proton and its closest electron only).

Rates do not change also with the increase of the intra-molecular protons n in Eqs. (S3) - (S6), since the term containing $\aleph_{(\text{HFC},\Sigma\text{HF}),\text{intra}}$ remains much smaller than the term containing Δ_{EE}^2 , Fig. S1.

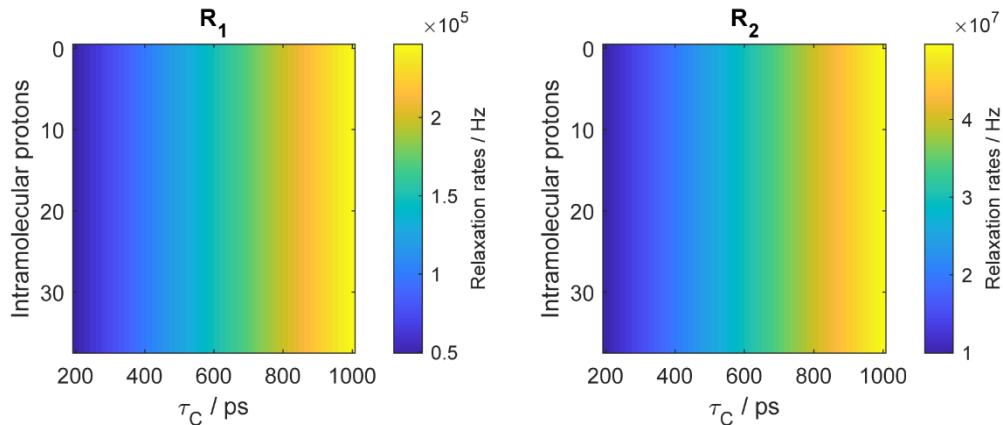


Fig. S1: R_1 and R_2 electron relaxation rates predicted by Eq. (S5) and Eq. (S6) as a function of τ_c and on the number of closest intramolecular protons n to an electron (36 in the case of a model bis-trityl). For these calculations J_{ex} was set equal to $\omega_E + \omega_N$, B_0 was set equal to 14.08 T, and other simulation parameters are as given in the Table 1. The absence of a strong dependence with the number of protons reflects the dominant effects of electron-electron dipole and g anisotropies on the relaxation processes, over hyperfine counterparts.

It is enlightening to consider how this model predicts the electron saturation and J-DNP enhancement to proceed, as a function of the available microwave power. Considering that the rotational correlation time of the trityl monomer is about 150 ps –calculated from $\tau_C \simeq r_D^2/D_t$ [3], where D_t is trityl’s translational diffusion constant (which ranges between $1.9 \times 10^{-9} \text{ m}^2 \text{ s}^{-1}$ and $2.7 \times 10^{-9} \text{ m}^2 \text{ s}^{-1}$) and r_D is the minimum distance approach between an electron in the biradical and a proton in the solvent (estimated at about 5-10 Å)– we decided to set the τ_C for the biradical as $\tau_C \approx 500$ ps. Figure S2 shows the predicted electron saturation and J-DNP enhancement effects expected for this τ_C as a function of microwave off-resonance offset and nutation field; similar enhancements and saturation behaviors are predicted for smaller and higher rotational correlation times, up to 1 ns.

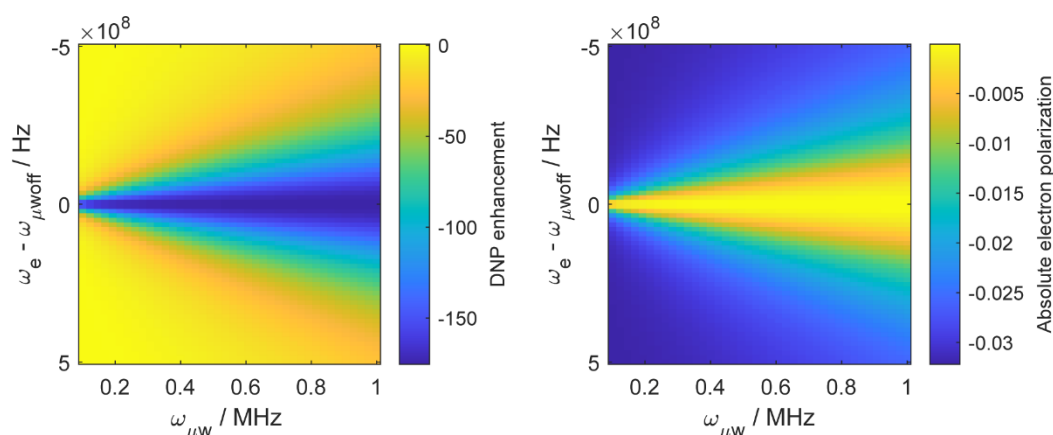


Fig. S2: Maximum enhancement (absolute value over the thermal equilibrium) in J-DNP (on the left), achieved around 100 ms, and absolute electron polarization, \hat{E}_Z , (on the right), as a function of μW frequency offset from the free electron Larmor frequency and of the μW nutation power, $\omega_{\mu\text{W}}$. For these calculations J_{ex} is equal to $\omega_E + \omega_N$, B_0 is 14.08 T, $\tau_C = 500$ ps, and other simulation parameters as given in the Table 1.

Supporting Information 2: The Hamiltonian Used in the Propagation of the Biradical/Nuclear System – From the Single-Spin to the Triplet-Singlet Representations

The laboratory frame Hamiltonian for a three-spin system composed by two electrons and one proton, where the electrons are connected by dipolar and exchange couplings, and the proton interacts with the electrons through hyperfine (dipolar) coupling only, can be written using single-spin Cartesian operators, as:

$$\hat{H}_{\text{lab.}} = \underbrace{\sum_k \hat{E}^{(k)} \cdot \mathbf{Z}_E^{(k)} \cdot \vec{B}_0 + \hat{N} \cdot \mathbf{Z}_N \cdot \vec{B}_0}_{\text{Zeeman interaction}} + \underbrace{\hat{E}^{(1)} \cdot (\mathbf{D} + J_{\text{ex}}) \cdot \hat{E}^{(2)}}_{\text{Dipolar and scalar inter-electron interaction}} + \underbrace{\sum_k \hat{E}^{(k)} \cdot \mathbf{A}^{(k)} \cdot \hat{N}}_{\text{Hyperfine interaction}} \quad (\text{S7})$$

where $\mathbf{Z}_E^{(k)}$ are the Zeeman tensors (including g-anisotropy) of electron spins $k=1,2$; \mathbf{Z}_N is the Zeeman tensor of the sole nuclear spin being considered (including the chemical shift anisotropy); \mathbf{D} is the inter-electron dipolar interaction tensor in the point magnetic dipole approximation; J_{ex} is the inter-electron scalar (*aka* “exchange”) coupling in angular frequency units; $\mathbf{A}^{(k)}$ is the hyperfine interaction tensors of the nucleus with the indicated electron k ; \vec{B}_0 is the external magnetic field; and $\hat{E}^{(1)}$, $\hat{E}^{(2)}$ and \hat{N} are the Cartesian spin-1/2 operators for the two electrons and nucleus. A rotating frame transformation with respect to the microwave frequency offset using the operator $\omega_{\mu\text{Woff}} \sum_k \hat{E}_Z^{(k)}$ and preservation of the usual secular and pseudosecular terms, leads to

$$\begin{aligned} \hat{H}_{rot.} = & \omega_{\Sigma e} (\hat{E}_{1Z} + \hat{E}_{2Z}) + \omega_{\Delta e} (\hat{E}_{1Z} - \hat{E}_{2Z}) + \omega_N \hat{N}_Z + \omega_1 \hat{E}_{1Z} \hat{E}_{2Z} + \omega_2 \left(\frac{\hat{E}_{1+} \hat{E}_{2-} + \hat{E}_{1-} \hat{E}_{2+}}{2} \right) \\ & + A_{\Sigma} (\hat{E}_{1Z} + \hat{E}_{2Z}) \hat{N}_Z + A_{\Delta} (\hat{E}_{1Z} - \hat{E}_{2Z}) \hat{N}_Z + B_{\Sigma} (\hat{E}_{1Z} + \hat{E}_{2Z}) \hat{N}_X + B_{\Delta} (\hat{E}_{1Z} - \hat{E}_{2Z}) \hat{N}_X \end{aligned} \quad (S8)$$

where $\omega_{\Sigma e}$ and $\omega_{\Delta e}$ are the sum and the difference between the rotating-frame offsets of the two electrons; $A_{\Sigma} = A_1 + A_2$ and $A_{\Delta} = A_1 - A_2$; $B_{\Sigma} = B_1 + B_2$ and $B_{\Delta} = B_1 - B_2$ are the sum and the difference of the secular and pseudo-secular coefficients describing the hyperfine interaction, respectively; and $\omega_1 = (J_{ex} + 2\mathbf{D})$ and $\omega_2 = (J_{ex} - \mathbf{D})$, where \mathbf{D} is the inter-electron dipolar interaction tensor. It is suitable to express the electronic components of this spin Hamiltonian in singlet – triplet state operators when $J_{ex} \approx \omega_E \gg \omega_{\Delta e}$, forming the natural spin space under such conditions. [4] The single-spin electron Cartesian operators in Eqs. (S7), (S8) can be transformed into a singlet-triplet basis set using fictitious $\frac{1}{2}$ -spin operators; [5, 6] since the addition of a third nuclear spin has to our knowledge not been reported before, we summarize in this Supplement how it leads to Eq. (3) of the main text. To do so we reexpress the rotating-frame Hamiltonian in Eq. (S8), as a sum of terms containing direct products of operators acting in the $S_0 T_0$ and the $T_{+1} T_{-1}$ electron subspaces, with the nuclear Zeeman base. The fictitious spin-1/2 operators that we use in this study to describe the $S_0 T_0$ and the $T_{+1} T_{-1}$ electron subspaces follow from Vega's notation for two-spin fictitious operators.[7] When adding to these direct products with the nuclear spin, the fictitious spin- $\frac{1}{2}$ operators for the electrons/nucleus in the $T_0 S_0$ subspace end up being:

$$\begin{aligned} L_X^{T_0 S_0, \alpha} &= \frac{1}{2} \left(|T_0^{(e1, e2)}, \alpha\rangle \langle S_0^{(e1, e2)}, \alpha| + |S_0^{(e1, e2)}, \alpha\rangle \langle T_0^{(e1, e2)}, \alpha| \right) \\ &= \frac{\hat{E}_{1Z}}{4} - \frac{\hat{E}_{2Z}}{4} + \frac{1}{2} (\hat{E}_{1Z} \hat{N}_Z) - \frac{1}{2} (\hat{E}_{2Z} \hat{N}_Z) \end{aligned} \quad (S9)$$

$$\begin{aligned} L_X^{T_0 S_0, \beta} &= \frac{1}{2} \left(|T_0^{(e1, e2)}, \beta\rangle \langle S_0^{(e1, e2)}, \beta| + |S_0^{(e1, e2)}, \beta\rangle \langle T_0^{(e1, e2)}, \beta| \right) \\ &= \frac{\hat{E}_{1Z}}{4} - \frac{\hat{E}_{2Z}}{4} - \frac{1}{2} (\hat{E}_{1Z} \hat{N}_Z) + \frac{1}{2} (\hat{E}_{2Z} \hat{N}_Z) \end{aligned} \quad (S10)$$

which we combine to obtain:

$$\omega_{\Delta e} (\hat{E}_{1Z} - \hat{E}_{2Z}) = 2\omega_{\Delta e} (L_X^{T_0 S_0, \alpha} + L_X^{T_0 S_0, \beta}) \quad (S11)$$

$$A_{\Delta} (\hat{E}_{1Z} N_Z - \hat{E}_{2Z} N_Z) = A_{\Delta} (L_X^{T_0 S_0, \alpha} - L_X^{T_0 S_0, \beta}) \quad (S12)$$

The longitudinal fictitious $\frac{1}{2}$ -spin operators for the electron in the $T_0 S_0$ are:

$$\begin{aligned} L_Z^{T_0 S_0, \alpha} &= \frac{1}{2} \left(|T_0^{(e1, e2)}, \alpha\rangle \langle T_0^{(e1, e2)}, \alpha| - |S_0^{(e1, e2)}, \alpha\rangle \langle S_0^{(e1, e2)}, \alpha| \right) \\ &= -\frac{1}{2} \hat{E}_{1X} \hat{E}_{2X} - \frac{1}{2} \hat{E}_{1Y} \hat{E}_{2Y} - \hat{E}_{1X} \hat{E}_{2X} \hat{N}_Z - \hat{E}_{1Y} \hat{E}_{2Y} \hat{N}_Z \end{aligned} \quad (S13)$$

$$\begin{aligned} L_Z^{T_0 S_0, \beta} &= \frac{1}{2} \left(|T_0^{(e1, e2)}, \beta\rangle \langle T_0^{(e1, e2)}, \beta| - |S_0^{(e1, e2)}, \beta\rangle \langle S_0^{(e1, e2)}, \beta| \right) \\ &= -\frac{1}{2} \hat{E}_{1X} \hat{E}_{2X} - \frac{1}{2} \hat{E}_{1Y} \hat{E}_{2Y} + \hat{E}_{1X} \hat{E}_{2X} \hat{N}_Z + \hat{E}_{1Y} \hat{E}_{2Y} \hat{N}_Z \end{aligned} \quad (S14)$$

$$\begin{aligned}\mathbf{E}^{T_0S_0,\alpha} &= \left(|T_0^{(e1,e2)}, \alpha\rangle \langle T_0^{(e1,e2)}, \alpha| + |S_0^{(e1,e2)}, \alpha\rangle \langle S_0^{(e1,e2)}, \alpha| \right) \\ &= -\hat{E}_{1Z}\hat{E}_{2Z} - 2\hat{E}_{1Z}\hat{E}_{2Z}\hat{N}_Z + \frac{1}{2}\hat{N}_Z + \frac{\mathbf{E}}{4}\end{aligned}\quad (\text{S15})$$

$$\begin{aligned}\mathbf{E}^{T_0S_0,\beta} &= \left(|T_0^{(e1,e2)}, \beta\rangle \langle T_0^{(e1,e2)}, \beta| + |S_0^{(e1,e2)}, \beta\rangle \langle S_0^{(e1,e2)}, \beta| \right) \\ &= -\hat{E}_{1Z}\hat{E}_{2Z} + 2\hat{E}_{1Z}\hat{E}_{2Z}\hat{N}_Z - \frac{1}{2}\hat{N}_Z + \frac{\mathbf{E}}{4}\end{aligned}\quad (\text{S16})$$

from which we obtain:

$$\omega_2 \left(L_Z^{T_0S_0,\alpha} + L_Z^{T_0S_0,\beta} \right) = \omega_2 \left(\hat{E}_{1X}\hat{E}_{2X} + \hat{E}_{1Y}\hat{E}_{2Y} \right) \quad (\text{S17})$$

$$\omega_1 \left(\frac{\mathbf{E}^{T_0S_0,\alpha} + \mathbf{E}^{T_0S_0,\beta}}{4} \right) = \omega_1 \left(-\frac{1}{2}\hat{E}_{1Z}\hat{E}_{2Z} + \frac{\mathbf{E}}{8} \right) \quad (\text{S18})$$

The transverse fictitious $\frac{1}{2}$ -spin operators for the proton in the T_0S_0 subspace are:

$$\begin{aligned}L_X^{S_0T_0,\alpha\beta} &= \frac{1}{2} \left(|S_0^{(e1,e2)}, \alpha\rangle \langle T_0^{(e1,e2)}, \beta| + |T_0^{(e1,e2)}, \beta\rangle \langle S_0^{(e1,e2)}, \alpha| \right) \\ &= \frac{1}{2}\hat{E}_{1Z}\hat{N}_X - \frac{1}{2}\hat{E}_{2Z}\hat{N}_X + \hat{E}_{1X}\hat{E}_{2Y}\hat{N}_Y - \hat{E}_{1Y}\hat{E}_{2X}\hat{N}_Y\end{aligned}\quad (\text{S19})$$

$$\begin{aligned}L_X^{T_0S_0,\alpha\beta} &= \frac{1}{2} \left(|T_0^{(e1,e2)}, \alpha\rangle \langle S_0^{(e1,e2)}, \beta| + |S_0^{(e1,e2)}, \beta\rangle \langle T_0^{(e1,e2)}, \alpha| \right) \\ &= \frac{1}{2}\hat{E}_{1Z}\hat{N}_X - \frac{1}{2}\hat{E}_{2Z}\hat{N}_X - \hat{E}_{1X}\hat{E}_{2Y}\hat{N}_Y + \hat{E}_{1Y}\hat{E}_{2X}\hat{N}_Y\end{aligned}\quad (\text{S20})$$

from which we obtain the pseudo-secular component:

$$B_\Delta \left(L_X^{S_0T_0,\alpha\beta} + L_X^{T_0S_0,\alpha\beta} \right) = B_\Delta \left(\hat{E}_{1Z} - \hat{E}_{2Z} \right) \hat{N}_X \quad (\text{S21})$$

Longitudinal fictitious $\frac{1}{2}$ -spin operators for the electron in the $T_{+1}T_{-1}$ subspace are:

$$\begin{aligned}L_Z^{T_+T_-, \alpha} &= \frac{1}{2} \left(|T_{+1}^{(e1,e2)}, \alpha\rangle \langle T_{+1}^{(e1,e2)}, \alpha| - |T_{-1}^{(e1,e2)}, \alpha\rangle \langle T_{-1}^{(e1,e2)}, \alpha| \right) \\ &= \frac{\hat{E}_{1Z}}{4} + \frac{\hat{E}_{2Z}}{4} + \frac{1}{2} \left(\hat{E}_{1Z}\hat{N}_Z \right) + \frac{1}{2} \left(\hat{E}_{2Z}\hat{N}_Z \right)\end{aligned}\quad (\text{S22})$$

$$\begin{aligned}L_Z^{T_+T_-, \beta} &= \frac{1}{2} \left(|T_{+1}^{(e1,e2)}, \beta\rangle \langle T_{+1}^{(e1,e2)}, \beta| - |T_{-1}^{(e1,e2)}, \beta\rangle \langle T_{-1}^{(e1,e2)}, \beta| \right) \\ &= \frac{\hat{E}_{1Z}}{4} + \frac{\hat{E}_{2Z}}{4} - \frac{1}{2} \left(\hat{E}_{1Z}\hat{N}_Z \right) - \frac{1}{2} \left(\hat{E}_{2Z}\hat{N}_Z \right)\end{aligned}\quad (\text{S23})$$

$$\begin{aligned}\mathbf{E}^{T_+T_-, \alpha} &= \left(|T_{+1}^{(e1,e2)}, \alpha\rangle \langle T_{+1}^{(e1,e2)}, \alpha| + |T_{-1}^{(e1,e2)}, \alpha\rangle \langle T_{-1}^{(e1,e2)}, \alpha| \right) \\ &= \hat{E}_{1Z}\hat{E}_{2Z} + 2\hat{E}_{1Z}\hat{E}_{2Z}\hat{N}_Z + \frac{\hat{N}_Z}{2} + \frac{\mathbf{E}}{4}\end{aligned}\quad (\text{S24})$$

$$\begin{aligned}
\mathbf{E}^{T_+T_-, \beta} &= \left(|T_{+1}^{(e1, e2)}, \beta\rangle \langle T_{+1}^{(e1, e2)}, \beta| + |T_{-1}^{(e1, e2)}, \beta\rangle \langle T_{-1}^{(e1, e2)}, \beta| \right) \\
&= \hat{E}_{1Z} \hat{E}_{2Z} - 2\hat{E}_{1Z} \hat{E}_{2Z} \hat{N}_Z - \frac{\hat{N}_Z}{2} + \frac{\mathbf{E}}{4}
\end{aligned} \tag{S25}$$

from which we obtain:

$$\omega_{\Sigma e} \left(\hat{E}_{1Z} + \hat{E}_{2Z} \right) = 2\omega_{\Sigma e} \left(L_Z^{T_+T_-, \alpha} + L_Z^{T_+T_-, \beta} \right) \tag{S26}$$

$$A_{\Sigma} \left(\hat{E}_{1Z} \hat{N}_Z + \hat{E}_{2Z} \hat{N}_Z \right) = A_{\Sigma} \left(L_Z^{T_+T_-, \alpha} - L_Z^{T_+T_-, \beta} \right) \tag{S27}$$

$$\omega_1 \left(\frac{1}{2} \hat{E}_{1Z} \hat{E}_{2Z} + \frac{\mathbf{E}}{8} \right) = \omega_1 \left(\frac{\mathbf{E}^{T_+T_-, \alpha} + \mathbf{E}^{T_+T_-, \beta}}{4} \right) \tag{S28}$$

Finally, we introduce new transverse fictitious $\frac{1}{2}$ -spin operators for the proton in the $T_{\pm 1}$ subspace given by:

$$\begin{aligned}
L_X^{T_+, \alpha\beta} &= \frac{1}{2} \left(|T_{+1}^{(e1, e2)}, \alpha\rangle \langle T_{+1}^{(e1, e2)}, \beta| + |T_{+1}^{(e1, e2)}, \beta\rangle \langle T_{+1}^{(e1, e2)}, \alpha| \right) \\
&= \frac{1}{2} \hat{E}_{1Z} \hat{N}_X + \frac{1}{2} \hat{E}_{2Z} \hat{N}_X + \hat{E}_{1Z} \hat{E}_{2Z} \hat{N}_X + \frac{\hat{N}_X}{4}
\end{aligned} \tag{S29}$$

$$\begin{aligned}
L_X^{T_-, \alpha\beta} &= \frac{1}{2} \left(|T_{-1}^{(e1, e2)}, \alpha\rangle \langle T_{-1}^{(e1, e2)}, \beta| + |T_{-1}^{(e1, e2)}, \beta\rangle \langle T_{-1}^{(e1, e2)}, \alpha| \right) \\
&= -\frac{1}{2} \hat{E}_{1Z} \hat{N}_X - \frac{1}{2} \hat{E}_{2Z} \hat{N}_X + \hat{E}_{1Z} \hat{E}_{2Z} \hat{N}_X + \frac{\hat{N}_X}{4}
\end{aligned} \tag{S30}$$

which are needed to describe the pseudo-secular component:

$$B_{\Sigma} \left(L_X^{T_+, \alpha\beta} - L_X^{T_-, \alpha\beta} \right) = B_{\Sigma} \left(\hat{E}_{1Z} + \hat{E}_{2Z} \right) \hat{N}_X \tag{S31}$$

The sum of these various terms, enables us to rewrite the Hamiltonian in Eq. (S8) as:

$$\begin{aligned}
\hat{H}_{rot} &= \hat{H}^{S_0T_0} + \hat{H}^{T_+T_-, \alpha\beta}, \text{ where:} \\
\hat{H}^{S_0T_0} &= 2\omega_{\Delta e} \left(L_X^{T_0S_0, \alpha} + L_X^{T_0S_0, \beta} \right) + A_{\Delta} \left(L_X^{T_0S_0, \alpha} - L_X^{T_0S_0, \beta} \right) + B_{\Delta} \left(L_X^{S_0T_0, \alpha\beta} + L_X^{T_0S_0, \alpha\beta} \right) \\
&\quad - \omega_2 \left(L_Z^{T_0S_0, \alpha} + L_Z^{T_0S_0, \beta} \right) - \omega_1 \left(\frac{\mathbf{E}^{T_0S_0, \alpha} + \mathbf{E}^{T_0S_0, \beta}}{4} \right), \\
\hat{H}^{T_+T_-, \alpha\beta} &= 2\omega_{\Sigma e} \left(L_Z^{T_+T_-, \alpha} + L_Z^{T_+T_-, \beta} \right) + \omega_N \hat{N}_Z + B_{\Sigma} \left(L_X^{T_+, \alpha\beta} - L_X^{T_-, \alpha\beta} \right) \\
&\quad + A_{\Sigma} \left(L_Z^{T_+T_-, \alpha} - L_Z^{T_+T_-, \beta} \right) + \omega_1 \left(\frac{\mathbf{E}^{T_+T_-, \alpha} + \mathbf{E}^{T_+T_-, \beta}}{4} \right)
\end{aligned} \tag{S32}$$

When adding to this expression the microwave irradiation Hamiltonian, Eq. (3a) of the main text is reached.

Supporting Information 3: Defining the Biradical/Nuclear System Populations Describing the J-DNP Enhancement

The main text defines $S_0 \hat{N}_Z$, $T_{\pm 1} \hat{N}_Z$ and $T_0 \hat{N}_Z$ operators, and relates these to the population differences leading to the predicted nuclear polarization enhancement. As these three-spin states

have to our knowledge not been previously defined, we summarize them here. To do this we rely again on Vega's two-spin triplet/single (TS) population operators, [5] and we direct-product them with a nuclear spin state that can be in either the α or β state. These can be written in terms of single-spin product operators, as:

$$S_{0,\alpha} = |S_0^{(e1,e2)}, \alpha\rangle \langle S_0^{(e1,e2)}, \alpha| = \frac{\mathbf{E}}{8} + \frac{\hat{N}_Z}{4} - \frac{1}{4}(\hat{E}_{1-}\hat{E}_{2+}) - \frac{1}{4}(\hat{E}_{1+}\hat{E}_{2-}) + \frac{1}{2}(\hat{E}_{1Z}\hat{E}_{2Z}) - \frac{1}{2}(\hat{E}_{1-}\hat{E}_{2+}\hat{N}_Z) - \frac{1}{2}(\hat{E}_{1+}\hat{E}_{2-}\hat{N}_Z) - \hat{E}_{1Z}\hat{E}_{2Z}\hat{N}_Z \quad (\text{S33})$$

$$T_{\pm 1,\alpha} = |T_{\pm 1}^{(e1,e2)}, \alpha\rangle \langle T_{\pm 1}^{(e1,e2)}, \alpha| = \frac{\mathbf{E}}{8} + \frac{\hat{N}_Z}{4} + \frac{\hat{E}_{1Z}}{4} \pm \frac{\hat{E}_{2Z}}{4} + \frac{1}{2}(\hat{E}_{1Z}\hat{E}_{2Z}) \pm \frac{1}{2}(\hat{E}_{1Z}\hat{N}_Z) \pm \frac{1}{2}(\hat{E}_{2Z}\hat{N}_Z) + \hat{E}_{1Z}\hat{E}_{2Z}\hat{N}_Z \quad (\text{S34})$$

$$T_{0,\alpha} = |T_0^{(e1,e2)}, \alpha\rangle \langle T_0^{(e1,e2)}, \alpha| = \frac{\mathbf{E}}{8} + \frac{\hat{N}_Z}{4} + \frac{1}{4}(\hat{E}_{1-}\hat{E}_{2+}) + \frac{1}{4}(\hat{E}_{1+}\hat{E}_{2-}) - \frac{1}{2}(\hat{E}_{1Z}\hat{E}_{2Z}) + \frac{1}{2}(\hat{E}_{1-}\hat{E}_{2+}\hat{N}_Z) + \frac{1}{2}(\hat{E}_{1+}\hat{E}_{2-}\hat{N}_Z) - \hat{E}_{1Z}\hat{E}_{2Z}\hat{N}_Z \quad (\text{S35})$$

$$S_{0,\beta} = |S_0^{(e1,e2)}, \beta\rangle \langle S_0^{(e1,e2)}, \beta| = \frac{\mathbf{E}}{8} - \frac{\hat{N}_Z}{4} - \frac{1}{4}(\hat{E}_{1-}\hat{E}_{2+}) - \frac{1}{4}(\hat{E}_{1+}\hat{E}_{2-}) + \frac{1}{2}(\hat{E}_{1Z}\hat{E}_{2Z}) + \frac{1}{2}(\hat{E}_{1-}\hat{E}_{2+}\hat{N}_Z) + \frac{1}{2}(\hat{E}_{1+}\hat{E}_{2-}\hat{N}_Z) + \hat{E}_{1Z}\hat{E}_{2Z}\hat{N}_Z \quad (\text{S36})$$

$$T_{\pm 1,\beta} = |T_{\pm 1}^{(e1,e2)}, \beta\rangle \langle T_{\pm 1}^{(e1,e2)}, \beta| = \frac{\mathbf{E}}{8} - \frac{\hat{N}_Z}{4} \pm \frac{\hat{E}_{1Z}}{4} \pm \frac{\hat{E}_{2Z}}{4} + \frac{1}{2}(\hat{E}_{1Z}\hat{E}_{2Z}) \mp \frac{1}{2}(\hat{E}_{1Z}\hat{N}_Z) \mp \frac{1}{2}(\hat{E}_{2Z}\hat{N}_Z) - \hat{E}_{1Z}\hat{E}_{2Z}\hat{N}_Z \quad (\text{S37})$$

$$T_{0,\beta} = |T_0^{(e1,e2)}, \beta\rangle \langle T_0^{(e1,e2)}, \beta| = \frac{\mathbf{E}}{8} - \frac{\hat{N}_Z}{4} + \frac{1}{4}(\hat{E}_{1-}\hat{E}_{2+}) + \frac{1}{4}(\hat{E}_{1+}\hat{E}_{2-}) - \frac{1}{2}(\hat{E}_{1Z}\hat{E}_{2Z}) - \frac{1}{2}(\hat{E}_{1-}\hat{E}_{2+}\hat{N}_Z) - \frac{1}{2}(\hat{E}_{1+}\hat{E}_{2-}\hat{N}_Z) + \hat{E}_{1Z}\hat{E}_{2Z}\hat{N}_Z \quad (\text{S38})$$

Taking suitable differences among these states, leads to the longitudinal fictitious operators used in the main text (e.g., Figures 4 and 5) to describe how singlet and triplet states enhance the nuclear polarization:

$$S_0^{(e1e2)}\hat{N}_Z = \frac{1}{2}(|S_0^{(e1e2)}, \alpha\rangle \langle S_0^{(e1e2)}, \alpha| - |S_0^{(e1e2)}, \beta\rangle \langle S_0^{(e1e2)}, \beta|) = \frac{\hat{N}_Z}{4} - \frac{1}{2}(\hat{E}_{1-}\hat{E}_{2+}\hat{N}_Z + \hat{E}_{1+}\hat{E}_{2-}\hat{N}_Z) - \hat{E}_{1Z}\hat{E}_{2Z}\hat{N}_Z \quad (\text{S39})$$

$$T_{\pm 1}^{(e1e2)}\hat{N}_Z = \frac{1}{2}(|T_{\pm 1}^{(e1e2)}, \alpha\rangle \langle T_{\pm 1}^{(e1e2)}, \alpha| - |T_{\pm 1}^{(e1e2)}, \beta\rangle \langle T_{\pm 1}^{(e1e2)}, \beta|) = \frac{\hat{N}_Z}{4} \pm \frac{1}{2}(\hat{E}_{1Z}\hat{N}_Z + \hat{E}_{2Z}\hat{N}_Z) + \hat{E}_{1Z}\hat{E}_{2Z}\hat{N}_Z \quad (\text{S40})$$

$$\begin{aligned}
T_0^{(e1e2)} \hat{N}_Z &= \frac{1}{2} \left(\left| T_0^{(e1e2)}, \alpha \right\rangle \left\langle T_0^{(e1e2)}, \alpha \right| - \left| T_0^{(e1e2)}, \beta \right\rangle \left\langle T_0^{(e1e2)}, \beta \right| \right) \\
&= \frac{\hat{N}_Z}{4} + \frac{1}{2} \left(\hat{E}_{1-} \hat{E}_{2+} \hat{N}_Z + \hat{E}_{1+} \hat{E}_{2-} \hat{N}_Z \right) - \hat{E}_{1Z} \hat{E}_{2Z} \hat{N}_Z
\end{aligned} \tag{S41}$$

Supporting Information 4: Additional Information about the Redfield Analysis of the Biradical/Nuclear System

The rate expressions derived by the Redfield theory analysis for the three-spin system in question (Eqs. (8)-(15) of the main text) were expressed on the basis of the square norms of second-rank 3x3 tensors:

$$\begin{aligned}
\aleph_{\mathbf{A},\mathbf{B}} &= \frac{\Delta_{\mathbf{A}+\mathbf{B}}^2 - \Delta_{\mathbf{A}-\mathbf{B}}^2}{4} \\
\Delta_{\mathbf{A}}^2 &= a_{XX}^2 + a_{YY}^2 + a_{ZZ}^2 - a_{XX}a_{YY} - a_{XX}a_{ZZ} - a_{YY}a_{ZZ} + \\
&\quad + \frac{3}{4} \left[(a_{XY} + a_{YX})^2 + (a_{XZ} + a_{ZX})^2 + (a_{YZ} + a_{ZY})^2 \right]
\end{aligned} \tag{S42}$$

where $\Delta_{\mathbf{A}}$ is the second-rank norm squared of a tensor \mathbf{A} and on the basis of the second-rank scalar product $\aleph_{\mathbf{A},\mathbf{B}}$ between two 3x3 interaction tensors \mathbf{A} and \mathbf{B} . The latter product can also contain linear combinations of more than two tensors; in Eqs. (8)-(15) of the main text and in the Supporting Information 5 section, these were often expressed based on the following algebraic relation:

$$\begin{aligned}
\Delta_{\mathbf{A}-\mathbf{B}}^2 &= \Delta_{\mathbf{A}}^2 + \Delta_{\mathbf{B}}^2 - 2\aleph_{\mathbf{A},\mathbf{B}}, \quad \Delta_{\mathbf{A}+\mathbf{B}}^2 = \Delta_{\mathbf{A}}^2 + \Delta_{\mathbf{B}}^2 + 2\aleph_{\mathbf{A},\mathbf{B}}, \\
\Delta_{\mathbf{A}+(\mathbf{B}+\mathbf{C})}^2 &= \Delta_{\mathbf{A}}^2 + \Delta_{\mathbf{B}+\mathbf{C}}^2 + 2\aleph_{\mathbf{A},\mathbf{B}+\mathbf{C}}, \quad \Delta_{\mathbf{A}-(\mathbf{B}+\mathbf{C})}^2 = \Delta_{\mathbf{A}}^2 + \Delta_{\mathbf{B}+\mathbf{C}}^2 - 2\aleph_{\mathbf{A},\mathbf{B}+\mathbf{C}}, \\
\Delta_{\mathbf{A}-\mathbf{B}}^2 &= \aleph_{\mathbf{A}-\mathbf{B},\mathbf{A}-\mathbf{B}}, \quad \Delta_{\mathbf{A}+\mathbf{B}}^2 = \aleph_{\mathbf{A}+\mathbf{B},\mathbf{A}+\mathbf{B}}, \\
\aleph_{\mathbf{A},\mathbf{B}+\mathbf{C}} &= \aleph_{\mathbf{A},\mathbf{B}} + \aleph_{\mathbf{A},\mathbf{C}}, \quad \aleph_{\mathbf{A},\mathbf{B}-\mathbf{C}} = \aleph_{\mathbf{A},\mathbf{B}} - \aleph_{\mathbf{A},\mathbf{C}}, \\
\aleph_{\mathbf{A}+(\mathbf{D}+\mathbf{E}),\mathbf{B}+\mathbf{C}} &= \aleph_{\mathbf{A},\mathbf{B}+\mathbf{C}} + \aleph_{\mathbf{D}+\mathbf{E},\mathbf{B}+\mathbf{C}}, \\
\aleph_{\mathbf{A}-\mathbf{D},\mathbf{B}+\mathbf{C}} &= \aleph_{\mathbf{A},\mathbf{B}+\mathbf{C}} + \aleph_{-\mathbf{D},\mathbf{B}+\mathbf{C}}, \\
\aleph_{\mathbf{A}-\mathbf{B},-(\mathbf{C}-\mathbf{D})} + \aleph_{\mathbf{A}-\mathbf{B},\mathbf{A}-\mathbf{B}} &= \aleph_{\mathbf{A}-\mathbf{B},(\mathbf{A}-\mathbf{B})-(\mathbf{C}-\mathbf{D})}, \quad \aleph_{\mathbf{A}+\mathbf{B},-(\mathbf{C}+\mathbf{D})} + \aleph_{\mathbf{A}+\mathbf{B},\mathbf{A}+\mathbf{B}} = \aleph_{\mathbf{A}+\mathbf{B},(\mathbf{A}+\mathbf{B})-(\mathbf{C}+\mathbf{D})} \\
\aleph_{\mathbf{A}-\mathbf{B},\mathbf{C}-\mathbf{D}} + \aleph_{\mathbf{A}-\mathbf{B},\mathbf{A}-\mathbf{B}} &= \aleph_{\mathbf{A}-\mathbf{B},(\mathbf{A}-\mathbf{B})+(\mathbf{C}-\mathbf{D})}, \quad \aleph_{\mathbf{A}+\mathbf{B},\mathbf{C}+\mathbf{D}} + \aleph_{\mathbf{A}+\mathbf{B},\mathbf{A}+\mathbf{B}} = \aleph_{\mathbf{A}+\mathbf{B},(\mathbf{A}+\mathbf{B})+(\mathbf{C}+\mathbf{D})}
\end{aligned} \tag{S43}$$

Supporting Information 5: Additional Redfield-derived Relaxation Rates for the Biradical/Nuclear System

The main text presented a simplified version of the rates of $S_{0,\alpha/\beta}$, $T_{0,\alpha/\beta}$, $T_{\pm 1,\alpha/\beta}$, whose full expressions are provided here. For $S_{0,\alpha/\beta}$ these were

$$\begin{aligned}
-R[S_{0,\beta}] &= \frac{\Delta_{\Delta\text{HF}}^2}{180} J(J_{\text{ex}} - \omega_{\text{E}} + \omega_{\text{N}}) + \frac{\Delta_{\Delta\text{HF}}^2}{30} J(J_{\text{ex}} + \omega_{\text{E}} + \omega_{\text{N}}) + \frac{\Delta_{\text{CSA}}^2}{15} J(\omega_{\text{N}}) + \frac{\Delta_{\Delta\text{HF}}^2}{60} J(J_{\text{ex}} + \omega_{\text{N}}) + \\
&\quad + \frac{[\Delta_{\Delta\text{HF}}^2 + 4\aleph_{\Delta\text{G},\Delta\text{G}-\Delta\text{HF}}]}{90} J(J_{\text{ex}}) + \frac{[\Delta_{\Delta\text{HF}}^2 + 4\aleph_{\Delta\text{G},\Delta\text{G}-\Delta\text{HF}}]}{120} J(J_{\text{ex}} - \omega_{\text{E}}) + \frac{[\Delta_{\Delta\text{HF}}^2 + 4\aleph_{\Delta\text{G},\Delta\text{G}-\Delta\text{HF}}]}{120} J(J_{\text{ex}} + \omega_{\text{E}})
\end{aligned} \tag{S44}$$

and

$$\begin{aligned}
-R[S_{0,\alpha}] &= \frac{\Delta_{\Delta HF}^2}{180} J(J_{\text{ex}} + \omega_E - \omega_N) + \frac{\Delta_{\Delta HF}^2}{30} J(J_{\text{ex}} - \omega_E - \omega_N) + \frac{\Delta_{\text{CSA}}^2}{15} J(\omega_N) + \frac{\Delta_{\Delta HF}^2}{60} J(J_{\text{ex}} - \omega_N) + \\
&+ \frac{[\Delta_{\Delta HF}^2 + 4\mathfrak{N}_{\Delta G, \Delta G + \Delta HF}]}{90} J(J_{\text{ex}}) + \frac{[\Delta_{\Delta HF}^2 + 4\mathfrak{N}_{\Delta G, \Delta G + \Delta HF}]}{120} J(J_{\text{ex}} - \omega_E) + \frac{[\Delta_{\Delta HF}^2 + 4\mathfrak{N}_{\Delta G, \Delta G + \Delta HF}]}{120} J(J_{\text{ex}} + \omega_E)
\end{aligned} \quad (\text{S45})$$

For the $T_{+1,\alpha/\beta}$ states these were:

$$\begin{aligned}
-R[T_{+1,\beta}] &= \frac{\Delta_{\Delta HF}^2}{180} J(J_{\text{ex}} + \omega_E - \omega_N) + \frac{[\Delta_{\Delta HF}^2 + 4\mathfrak{N}_{\Delta G, \Delta G - \Delta HF}]}{120} J(J_{\text{ex}} + \omega_E) + \\
&+ \frac{[\Delta_{\Sigma HF}^2 + 4\mathfrak{N}_{\text{CSA}, \text{CSA} + \Sigma HF}]}{60} J(\omega_N) + \frac{[5\Delta_{\Sigma HF}^2 + 12\mathfrak{N}_{\text{EE} + \Sigma G, (\text{EE} + \Sigma G) - \Sigma HF}]}{360} J(\omega_E) + \frac{\Delta_{\text{EE}}^2}{15} J(2\omega_E)
\end{aligned} \quad (\text{S46})$$

and

$$\begin{aligned}
-R[T_{+1,\alpha}] &= \frac{\Delta_{\Delta HF}^2}{30} J(J_{\text{ex}} + \omega_E + \omega_N) + \frac{[\Delta_{\Delta HF}^2 + 4\mathfrak{N}_{\Delta G, \Delta G + \Delta HF}]}{120} J(J_{\text{ex}} + \omega_E) + \\
&+ \frac{[\Delta_{\Sigma HF}^2 + 4\mathfrak{N}_{\text{CSA}, \text{CSA} + \Sigma HF}]}{60} J(\omega_N) + \frac{[5\Delta_{\Sigma HF}^2 + 4\mathfrak{N}_{\text{EE} + \Sigma G, (\text{EE} + \Sigma G) + \Sigma HF}]}{120} J(\omega_E) + \frac{\Delta_{\text{EE}}^2}{15} J(2\omega_E)
\end{aligned} \quad (\text{S47})$$

For the $T_{0,\alpha/\beta}$, the self-relaxation rates are

$$\begin{aligned}
-R[T_{0,\beta}] &= \frac{\Delta_{\text{CSA}}^2}{15} J(\omega_N) + \frac{\Delta_{\Delta HF}^2}{60} J(J_{\text{ex}} - \omega_N) + \\
&+ \frac{[\Delta_{\Delta HF}^2 + 4\mathfrak{N}_{\Delta G, \Delta G - \Delta HF}]}{90} J(J_{\text{ex}}) + \frac{[6\Delta_{\text{EE}}^2 + 5\Delta_{\Sigma HF}^2 + 6\mathfrak{N}_{\Sigma G, \Sigma G - \Sigma HF}]}{90} J(\omega_E)
\end{aligned} \quad (\text{S48})$$

and

$$\begin{aligned}
-R[T_{0,\alpha}] &= \frac{\Delta_{\text{CSA}}^2}{15} J(\omega_N) + \frac{\Delta_{\Delta HF}^2}{60} J(J_{\text{ex}} + \omega_N) + \\
&+ \frac{[\Delta_{\Delta HF}^2 + 4\mathfrak{N}_{\Delta G, \Delta G + \Delta HF}]}{90} J(J_{\text{ex}}) + \frac{[6\Delta_{\text{EE}}^2 + 5\Delta_{\Sigma HF}^2 + 6\mathfrak{N}_{\Sigma G, \Sigma G + \Sigma HF}]}{90} J(\omega_E)
\end{aligned} \quad (\text{S49})$$

And for $T_{-1,\alpha/\beta}$ the self-relaxation rates were:

$$\begin{aligned}
-R[T_{-1,\beta}] &= \frac{\Delta_{\Delta HF}^2}{30} J(J_{\text{ex}} - \omega_E - \omega_N) + \frac{[\Delta_{\Delta HF}^2 + 4\mathfrak{N}_{\Delta G, \Delta G - \Delta HF}]}{120} J(J_{\text{ex}} - \omega_E) + \\
&+ \frac{[\Delta_{\Sigma HF}^2 + 4\mathfrak{N}_{\text{CSA}, \text{CSA} - \Sigma HF}]}{60} J(\omega_N) + \frac{[5\Delta_{\Sigma HF}^2 + 4\mathfrak{N}_{\text{EE} - \Sigma G, \text{EE} - \Sigma G + \Sigma HF}]}{120} J(\omega_E) + \frac{\Delta_{\text{EE}}^2}{15} J(2\omega_E)
\end{aligned} \quad (\text{S50})$$

and

$$\begin{aligned}
-R[T_{-1,\alpha}] &= \frac{\Delta_{\Delta HF}^2}{180} J(J_{\text{ex}} - \omega_E + \omega_N) + \frac{[\Delta_{\Delta HF}^2 + 4\mathfrak{N}_{\Delta G, \Delta G + \Delta HF}]}{120} J(J_{\text{ex}} - \omega_E) + \\
&+ \frac{[\Delta_{\Sigma HF}^2 + 4\mathfrak{N}_{\text{CSA}, \text{CSA} - \Sigma HF}]}{60} J(\omega_N) + \frac{[5\Delta_{\Sigma HF}^2 + 12\mathfrak{N}_{\text{EE} - \Sigma G, \text{EE} - \Sigma G - \Sigma HF}]}{360} J(\omega_E) + \frac{\Delta_{\text{EE}}^2}{15} J(2\omega_E)
\end{aligned} \quad (\text{S51})$$

These expressions were all derived taking the possibility of having the spins' relaxation driven by the nuclear chemical shift anisotropy tensor (**CSA**), by $\Delta \mathbf{G} = \mathbf{G}_1 - \mathbf{G}_2$ and by $\Delta \mathbf{HF} = \mathbf{HFC}_1 - \mathbf{HFC}_2$ anisotropies deriving from tensors associated to the differences between the two g- and electron/nuclear hyperfine coupling tensors, respectively; by tensors $\Sigma \mathbf{G} = \mathbf{G}_1 + \mathbf{G}_2$ and $\Sigma \mathbf{HF} = \mathbf{HFC}_1 + \mathbf{HFC}_2$ associated to the sums of these two electronic g- and hyperfine tensors, and by the **EE** interaction representing the dipolar tensor between the two electrons (see footnote 2 in Table 1

regarding J_{ex} -driven scalar relaxation of the first kind). As is usual in spin relaxation theory [8, 9], all these rates contain combinations of second-rank norms squared $\Delta_{\mathbf{A}}^2$ of all the aforementioned tensors \mathbf{A} , second-rank scalar products $\aleph_{\mathbf{A},\mathbf{B}}$ of 3x3 tensors \mathbf{A} and \mathbf{B} [10], and linear combinations of these products among various tensors, as given in Supporting Information 4. Figures S3 and S4 below expand this matter further, by showing how rates of the α and β states direct-producing S_0 , T_0 and $T_{\pm 1}$ vary, when J_{ex} matches $\pm(\omega_{\text{E}} + \omega_{\text{N}})$ –this time as a function of B_0 and τ_{c} . Notice how these rates decrease with magnetic field and change differentially for α/β states with the correlation time. The main text presented how the rates of $S_{0,\alpha/\beta}$, $T_{0,\alpha/\beta}$, $T_{\pm 1,\alpha/\beta}$, changed with exchange coupling and magnetic field, according to numerical and analytical predictions (Fig. 5). Figures S3 and S4 below expand this matter further, by showing how rates of the α and β states direct-producing S_0 , T_0 and $T_{\pm 1}$ vary, when J_{ex} matches $\pm(\omega_{\text{E}} + \omega_{\text{N}})$ –this time as a function of B_0 and τ_{c} . Notice how these rates decrease with magnetic field and change differentially for α/β states with the correlation time.

The main text also presented the relaxation rates derived on the basis of Redfield's relaxation matrix for certain populations of relevance in the J-DNP process, based on the α and β nuclear states. For completion this section derives the expressions predicted by this theory, for the $\hat{N}_{\text{Z}}T_{\pm 1}$, $\hat{N}_{\text{Z}}T_0$ and $S_0\hat{N}_{\text{Z}}$ states.

$$\begin{aligned}
-R[\hat{N}_{\text{Z}}S_0] &= \frac{2\Delta_{\text{CSA}}^2}{15} J(\omega_{\text{N}}) + \frac{\Delta_{\text{AHF}}^2}{120} [J(J_{\text{ex}} - \omega_{\text{N}}) + J(J_{\text{ex}} + \omega_{\text{N}})] + \\
&+ \frac{\Delta_{\text{AHF}}^2}{60} [J(J_{\text{ex}} - \omega_{\text{E}} - \omega_{\text{N}}) + J(J_{\text{ex}} + \omega_{\text{E}} + \omega_{\text{N}})] + \\
&+ \frac{\Delta_{\text{AHF}}^2}{360} [J(J_{\text{ex}} + \omega_{\text{E}} - \omega_{\text{N}}) + J(J_{\text{ex}} - \omega_{\text{E}} + \omega_{\text{N}})] + \\
&+ \frac{\Delta_{\text{AHF}}^2 + 4\Delta_{\text{AG}}^2}{90} J(J_{\text{ex}}) + \frac{\Delta_{\text{AHF}}^2 + 4\Delta_{\text{AG}}^2}{120} [J(J_{\text{ex}} - \omega_{\text{E}}) + J(J_{\text{ex}} + \omega_{\text{E}})]
\end{aligned} \tag{S52}$$

$$\begin{aligned}
-R[\hat{N}_{\text{Z}}T_{+1}] &= \frac{\Delta_{\text{EE}}^2}{15} J(2\omega_{\text{E}}) + \frac{\Delta_{\text{AHF}}^2}{360} J(J_{\text{ex}} + \omega_{\text{E}} - \omega_{\text{N}}) + \frac{\Delta_{\text{AHF}}^2}{60} J(J_{\text{ex}} + \omega_{\text{E}} + \omega_{\text{N}}) + \\
&\frac{\Delta_{\text{AHF}}^2 + 4\Delta_{\text{AG}}^2}{120} J(J_{\text{ex}} + \omega_{\text{E}}) + \frac{[\Delta_{\text{SHF}}^2 + 4\aleph_{\text{CSA,CSA}+\text{SHF}}]}{30} J(\omega_{\text{N}}) + \frac{[5\Delta_{\text{SHF}}^2 + 6\Delta_{\text{EE}+\text{SG}}^2]}{180} J(\omega_{\text{E}})
\end{aligned} \tag{S53}$$

$$\begin{aligned}
-R[\hat{N}_{\text{Z}}T_{-1}] &= \frac{\Delta_{\text{EE}}^2}{15} J(2\omega_{\text{E}}) + \frac{\Delta_{\text{AHF}}^2}{360} J(J_{\text{ex}} - \omega_{\text{E}} + \omega_{\text{N}}) + \frac{\Delta_{\text{AHF}}^2}{60} J(J_{\text{ex}} - \omega_{\text{E}} - \omega_{\text{N}}) + \\
&\frac{\Delta_{\text{AHF}}^2 + 4\Delta_{\text{AG}}^2}{120} J(J_{\text{ex}} - \omega_{\text{E}}) + \frac{[\Delta_{\text{SHF}}^2 + 4\aleph_{\text{CSA,CSA}-\text{SHF}}]}{30} J(\omega_{\text{N}}) + \frac{[5\Delta_{\text{SHF}}^2 + 6\Delta_{\text{EE}-\text{SG}}^2]}{180} J(\omega_{\text{E}})
\end{aligned} \tag{S54}$$

$$\begin{aligned}
-R[\hat{N}_{\text{Z}}T_0] &= \frac{2\Delta_{\text{CSA}}^2}{15} J(\omega_{\text{N}}) + \frac{\Delta_{\text{AHF}}^2}{120} [J(J_{\text{ex}} - \omega_{\text{N}}) + J(J_{\text{ex}} + \omega_{\text{N}})] + \\
&+ \frac{\Delta_{\text{AHF}}^2 + 4\Delta_{\text{AG}}^2}{90} J(J_{\text{ex}}) + \frac{[6\Delta_{\text{EE}}^2 + 5\Delta_{\text{SHF}}^2 + 6\Delta_{\text{SG}}^2]}{90} J(\omega_{\text{E}})
\end{aligned} \tag{S55}$$

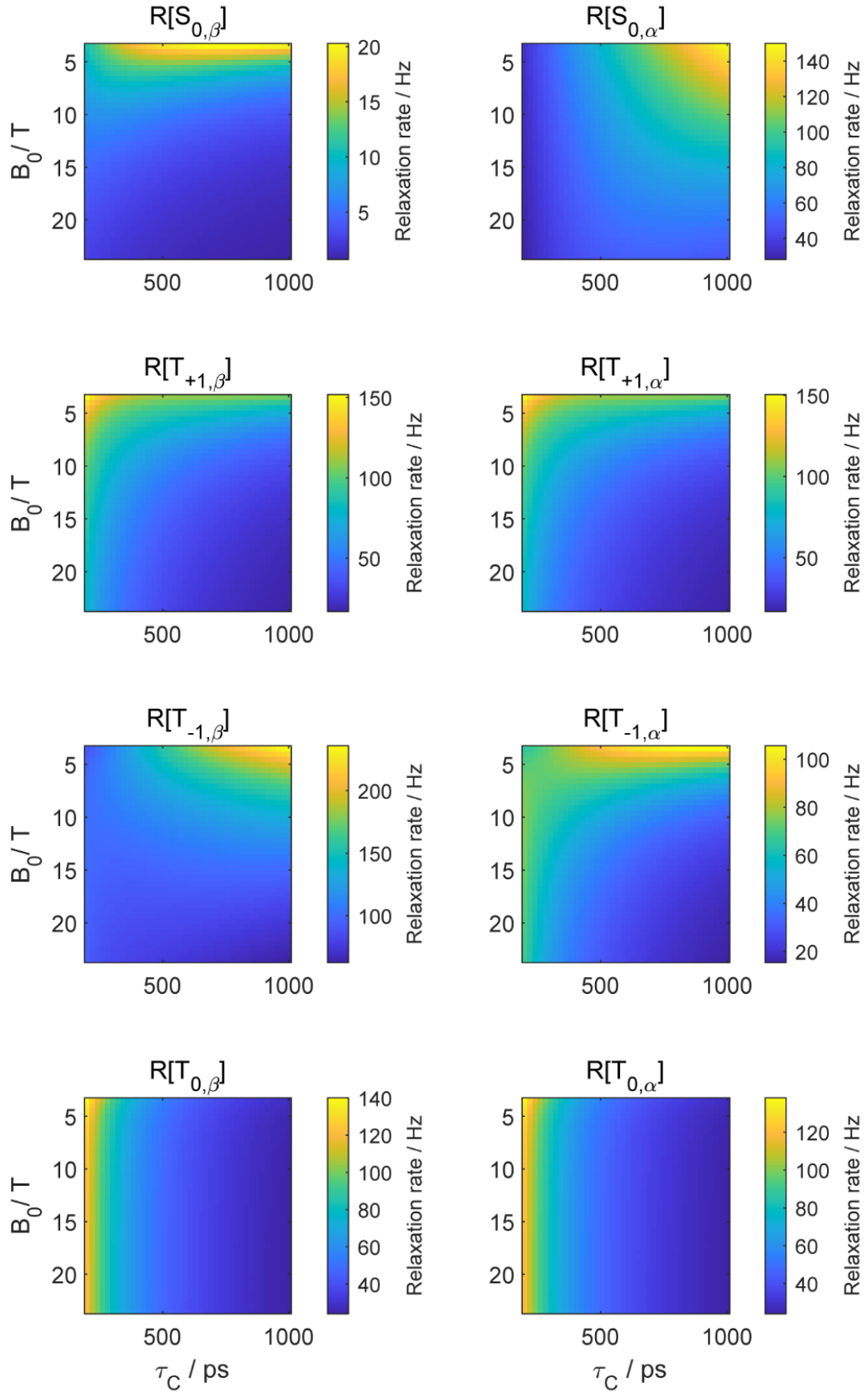


Fig. S3: Numerically calculated self-relaxation rates of $S_{0,\alpha/\beta}$, $T_{\pm 1,\alpha/\beta}$ and $T_{0,\alpha/\beta}$ as a function of B_0 and of τ_C , when J_{ex} is positive and equal to $J_{ex} = -(\omega_E + \omega_N)$. Other simulation parameters are given in Table 1.

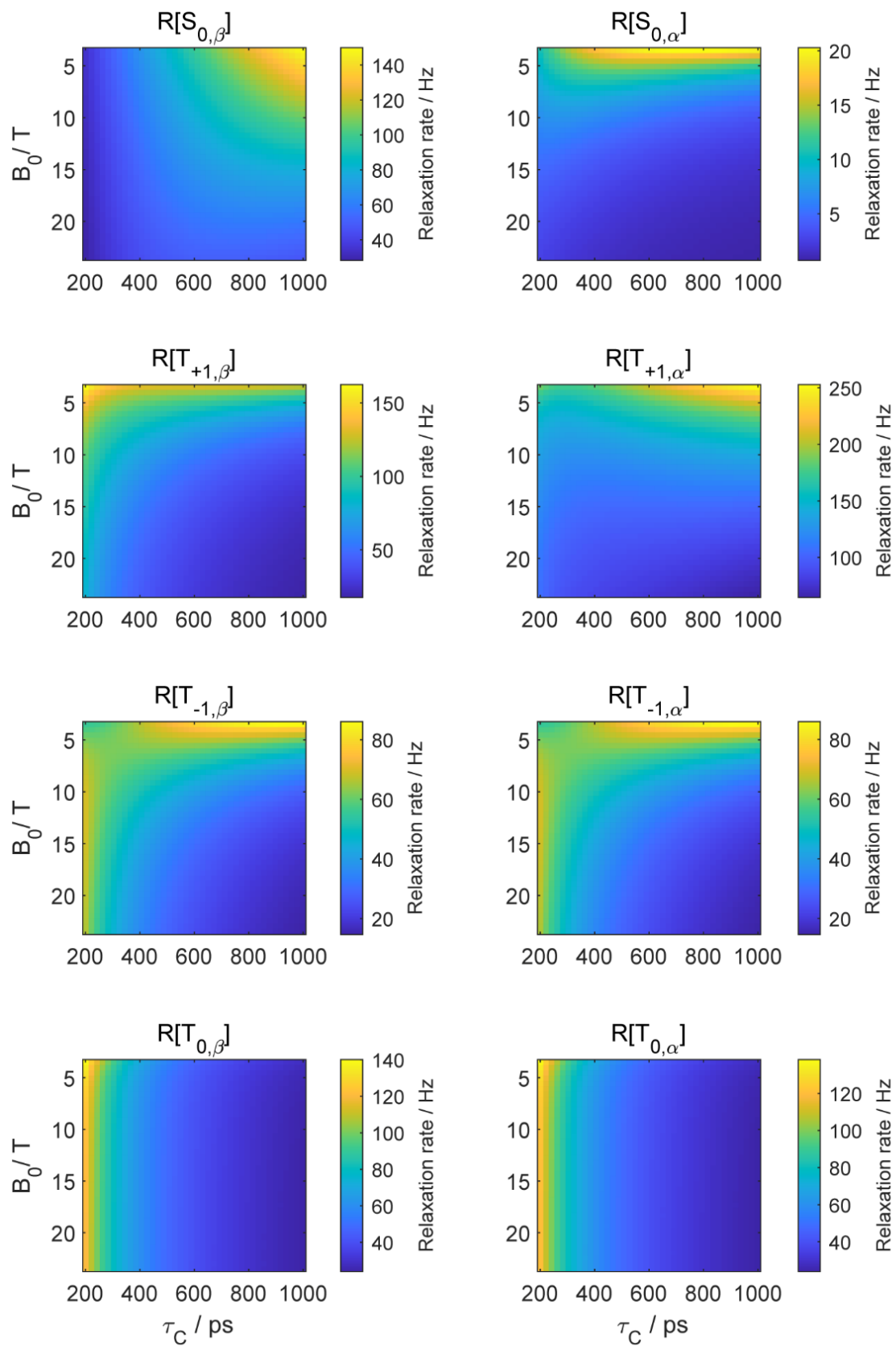


Fig. S4: Numerically calculated self-relaxation rates of $S_{0,\alpha/\beta}$, $T_{\pm 1,\alpha/\beta}$ and $T_{0,\alpha/\beta}$ as a function of B_0 and of τ_C , when J_{ex} is negative and equal to $J_{\text{ex}} = (\omega_E + \omega_N)$. Other simulation parameters are given in Table 1.

where the meaning of the various constants and functions are as in Eqs. (S44) - (S51) of the main text. Supporting Information Figures S5 and S6 present how these rates depend on B_0 and J_{ex} strengths, over a range of relevant values and correlation times.

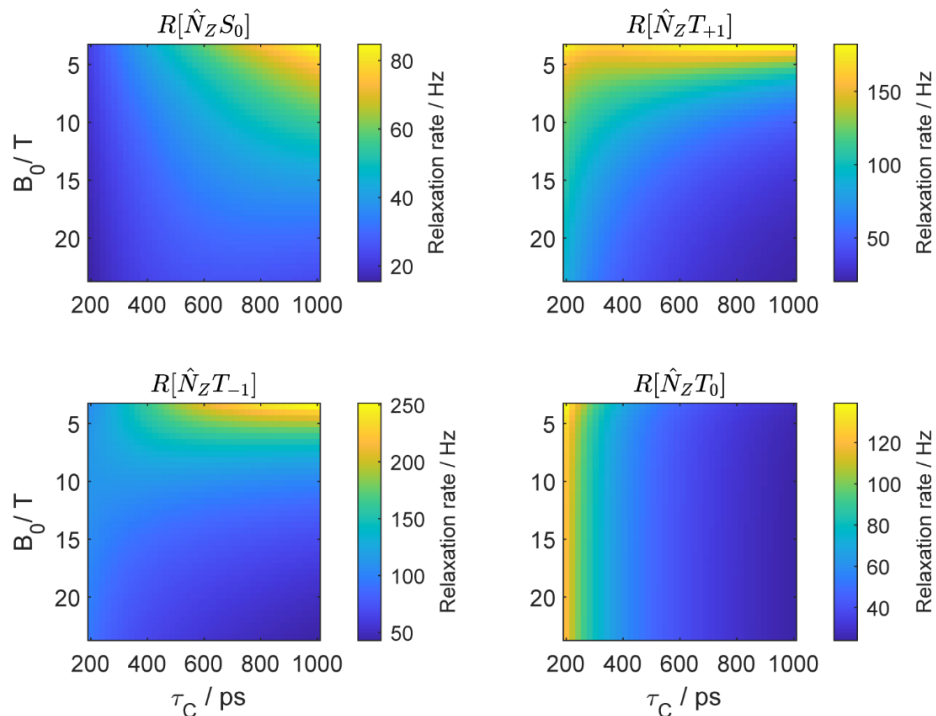


Fig. S5: Self-relaxation rates of $\hat{N}_Z S_0$, $\hat{N}_Z T_{\pm 1}$ and $\hat{N}_Z T_0$ states calculated as a function of B_0 and τ_C , for $J_{ex} = -(\omega_E + \omega_N)$. Other simulation parameters are given in Table 1.

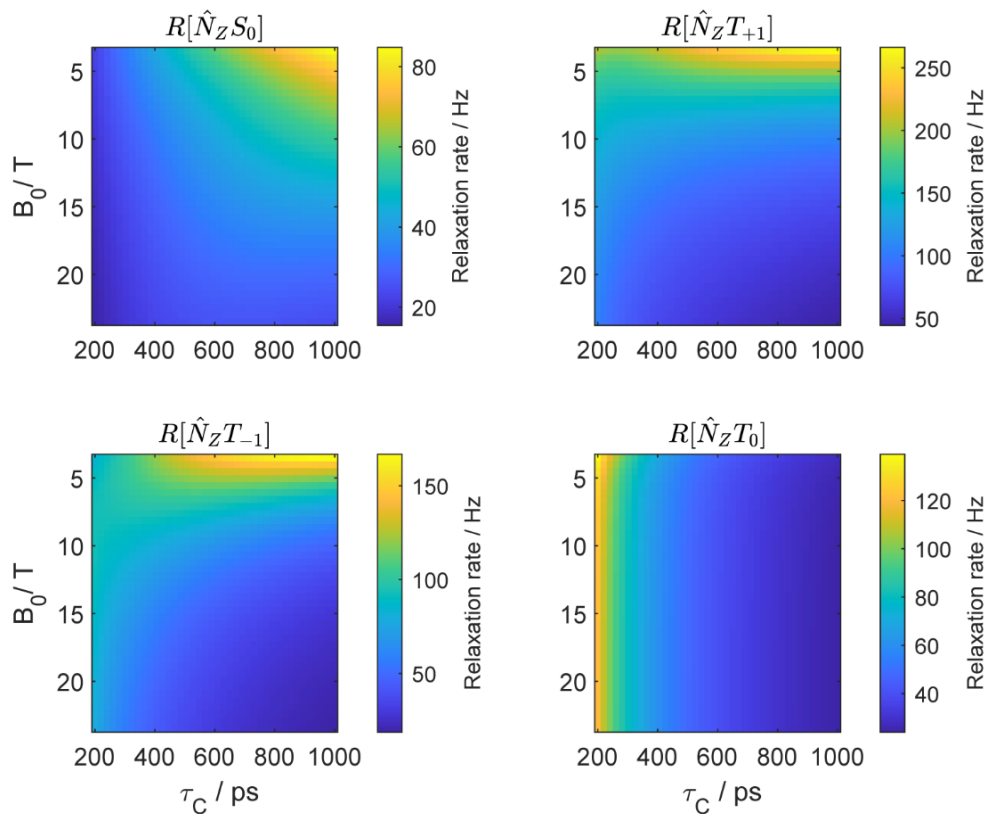


Fig. S6: Self-relaxation rates of $\hat{N}_Z S_0$, $\hat{N}_Z T_{\pm 1}$ and $\hat{N}_Z T_0$ states calculated as a function of B_0 and of τ_C , at $J_{ex} = +(\omega_E + \omega_N)$. Other simulation parameters are given in Table 1.

Supporting Information 6: J-DNP Enhancements for other kinds of biradical/nuclear systems

Table 1 in the main text focused on one combination of electronic and nuclear spin coupling parameters, leading to the features noted in the paper. This Section summarized three additional sets of combinations, as per the parameters summarized in Table S2. These include (i) the same coupling parameters as in Table 1 but for a different placement of the nucleus, which was now assumed devoid of chemical shift anisotropy; (ii) same parameters as in Table 1 but now with electronic sites endowed with identical rhombic g-tensors; (iii) same parameters as in Table 1 but now with the electrons devoid of g-anisotropies; (iv) same parameters as in Table 1 but now with electronic sites endowed with different isotropic g-tensors. The systems in the Table S2 thus contain axial, rhombic and isotropic g-tensors –in the latter case with coinciding and non-coinciding isotropic values. For the sake of conciseness, only the time-domain J-DNP transient enhancements were calculated for these scenarios –using the single optimal $J_{ex} = (\omega_E + \omega_N)$ but as function of B_0 field and correlation time. These are shown in Supporting Information Figures S7-S10. Note how similar is the behaviour for all these systems, when compared with that shown in Figure 2.

Table S3: Biradical / proton magnetic resonance parameters used in the simulations shown in Figures S7-S9. Each electron in the biradical had its parameters modelled on a trityl center, and the nucleus was placed along the linker closer to one of the electrons. B_0 , J_{ex} and τ_c were set as described in the figures; all other hyperfine coupling parameters relied on the distances.

Parameter	System i	System ii	System iii	System iv
^1H chemical shift tensor, ppm	[10 10 10]	[5 10 20]	[5 10 20]	[5 10 20]
g-tensor ¹ for the electron 1 and 2, Bohr magneton	[2.0032 2.0032 2.0026]	[2.0030 2.0025 2.0020]	[2.0032 2.0032 2.0032]	$g_1=[2.0032$ 2.0032 2.0032] $g_2=[2.0027$ 2.0027 2.0027]
^1H coordinates, [x y z], Å	[-3 0.5 1.3]	[-3 0.5 1.3]	[-3 0.5 1.3]	[-3 0.5 1.3]
Electron 1 coordinates, [x y z], Å	[0 0 -9.37]	[0 0 -9.37]	[0 0 -9.37]	[0 0 -9.37]
Electron 2 coordinates, [x y z], Å	[0 0 9.37]	[0 0 9.37]	[0 0 9.37]	[0 0 9.37]
Scalar relaxation modulation depth /GHz	3	3	3	1
Scalar relaxation modulation time, ps	1	1	1	1
Temperature/ K	298	298	298	298

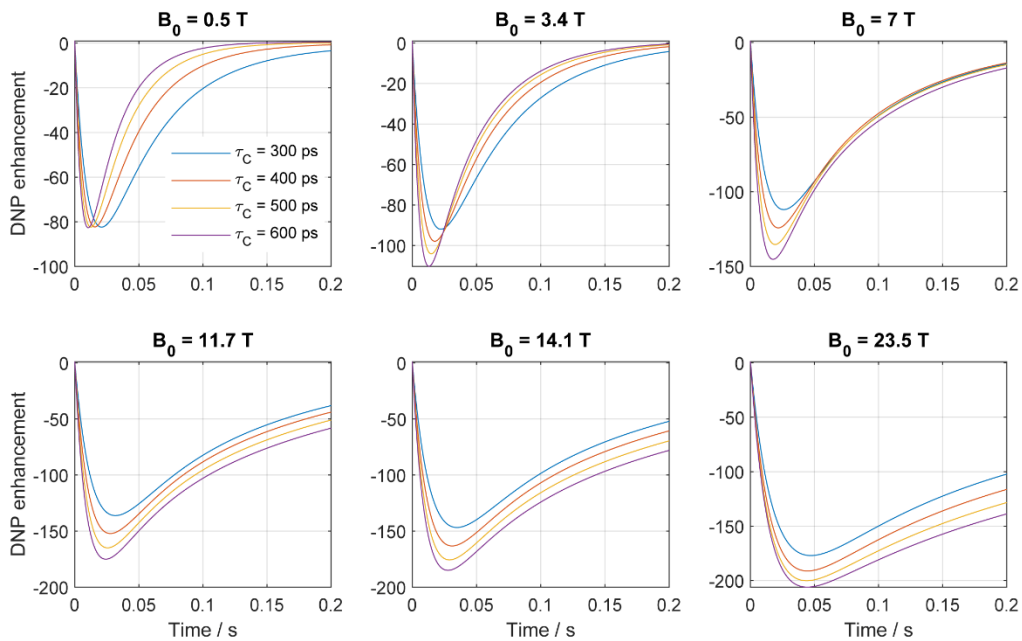


Fig. S7: Time domain simulations showing the evolution of the transient J-DNP enhancement as a function of B_0 and of τ_C . For all fields J_{ex} was tuned to $\omega_E + \omega_N$, using the parameters of the system (i) in Table S3.

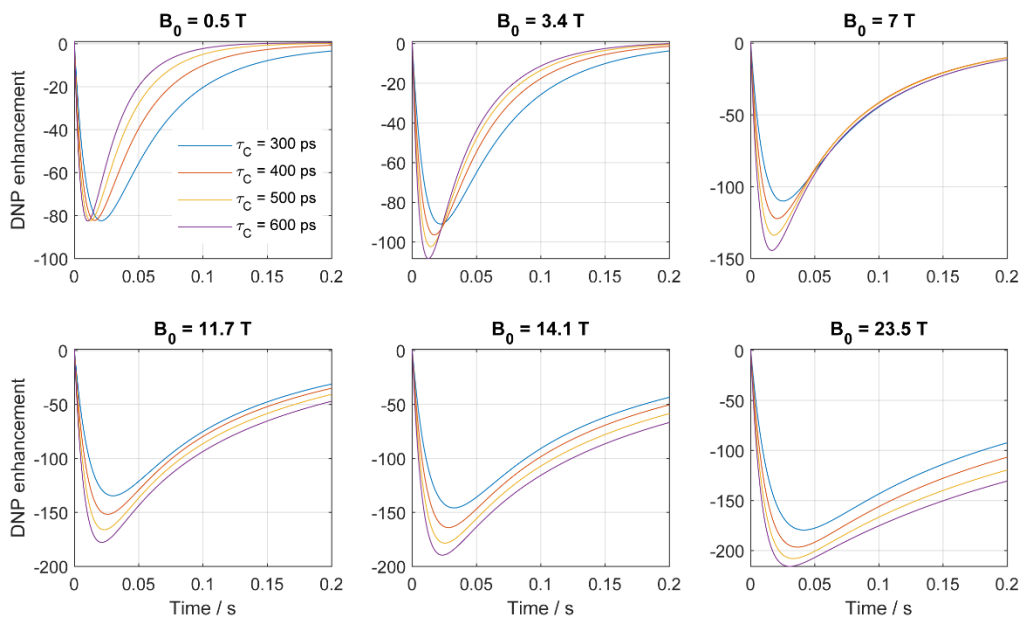


Fig. S8: Time domain simulations showing the evolution of the transient J-DNP enhancement as a function of B_0 and of τ_C . For all fields J_{ex} was tuned to $\omega_E + \omega_N$, using the parameters of the system (ii) in Table S3.

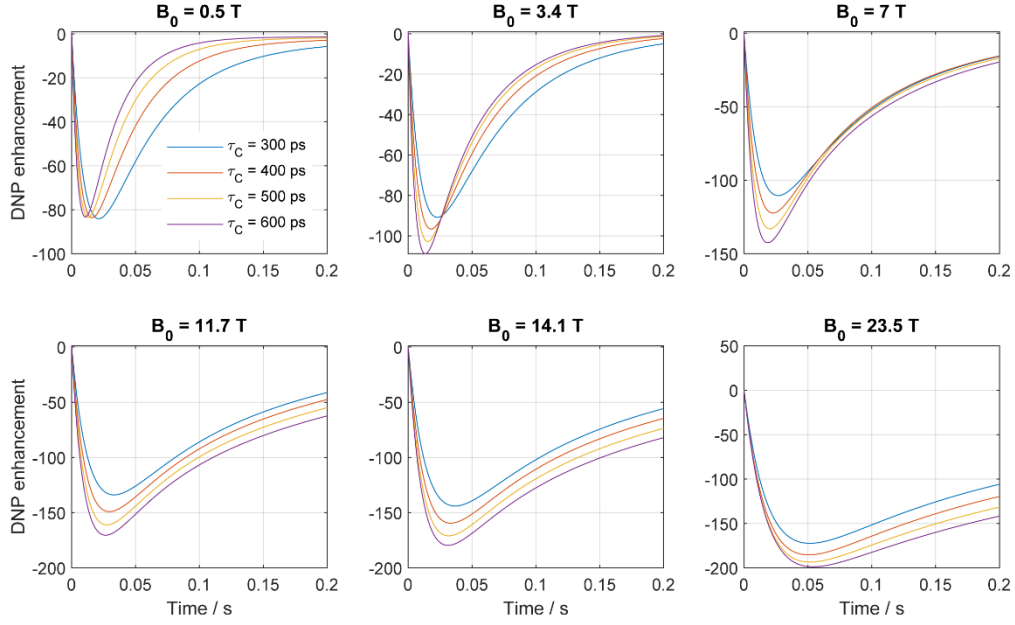


Fig. S9: Time domain simulations showing the evolution of the transient J-DNP enhancement as a function of B_0 and of τ_C . For all fields J_{ex} was tuned to $\omega_E + \omega_N$, using the parameters of the system (iii) in Table S3.

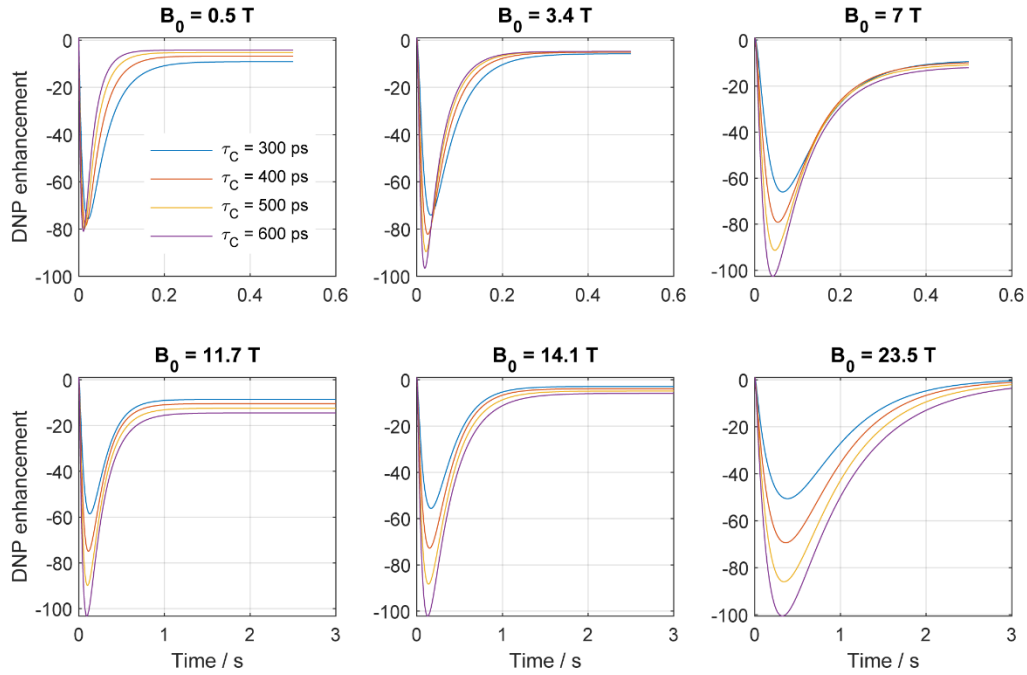


Fig. S10: Time domain simulations showing the evolution of the transient J-DNP enhancement as a function of B_0 and of τ_C . For all fields J_{ex} was tuned to $\omega_E + \omega_N$, using the parameters of the system (iv) in Table S3.

Despite the noted similarity among all these cases, it is important to remark that cases will also arise where the J-DNP enhancement will be “killed”. Figures S11 and S12 include two such instances. In the first of these the nucleus is symmetrically placed in-between two identical electrons that would otherwise lead to enhancement (i.e., Table 1 parameters); this makes the differential “CIDNP-like” effect stop working. The second case involves two electronic sites endowed with different anisotropic g -tensors; in such instance $\mathfrak{N}_{\Delta G, \Delta G \pm \Delta HF}$ – driven relaxation terms overtake the Δ_{HFC}^2 in Eqs. (8) – (15), robbing J-DNP for its efficiency even when $J_{ex} = \pm (\omega_E + \omega_N)$. Notice that this does not happen when $g_{1,iso} = g_{2,iso}$ (Fig. S10), as the $\mathfrak{N}_{\Delta G, \Delta G \pm \Delta HF}$ terms still remain then smaller than Δ_{HFC}^2 . Finally, another

instance were the effect decays to zero was noted in Figure 6 of the main text, and involved cases where the nucleus was too distant from the biradical.

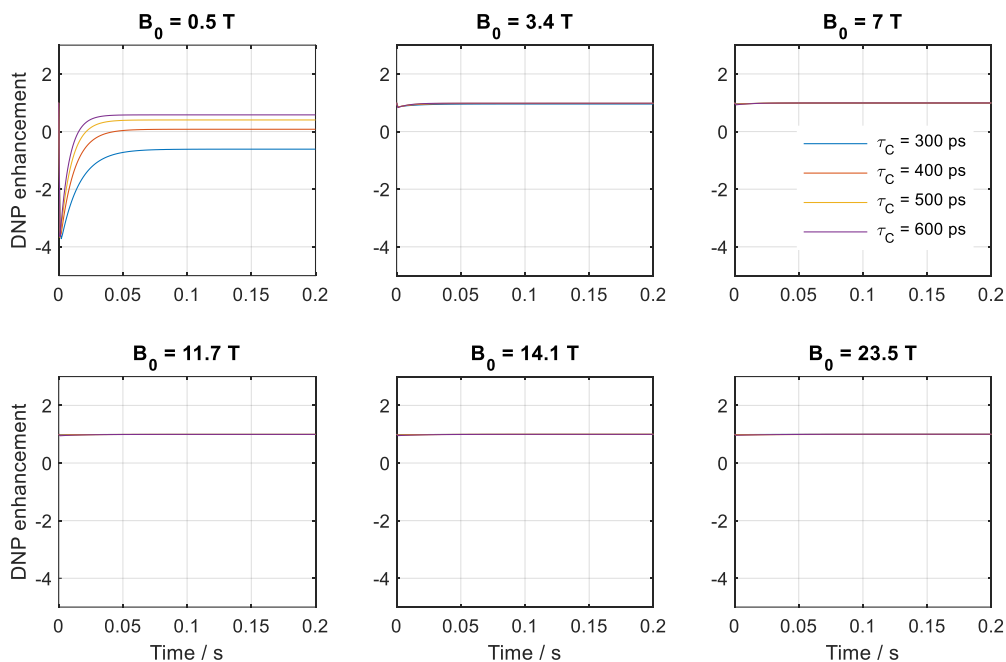


Fig. S11: Time domain simulations showing the evolution of the transient J-DNP enhancement as a function of B_0 and of τ_C . For all fields J_{ex} was tuned to $\omega_E + \omega_N$, using the same parameters as in Table 1 but now with electronic sites endowed with different anisotropic g -tensors equal to: $g_1=[2.0032 \ 2.0032 \ 2.0026]$ and $g_2=[2.0032 \ 2.0032 \ 2.0023]$.

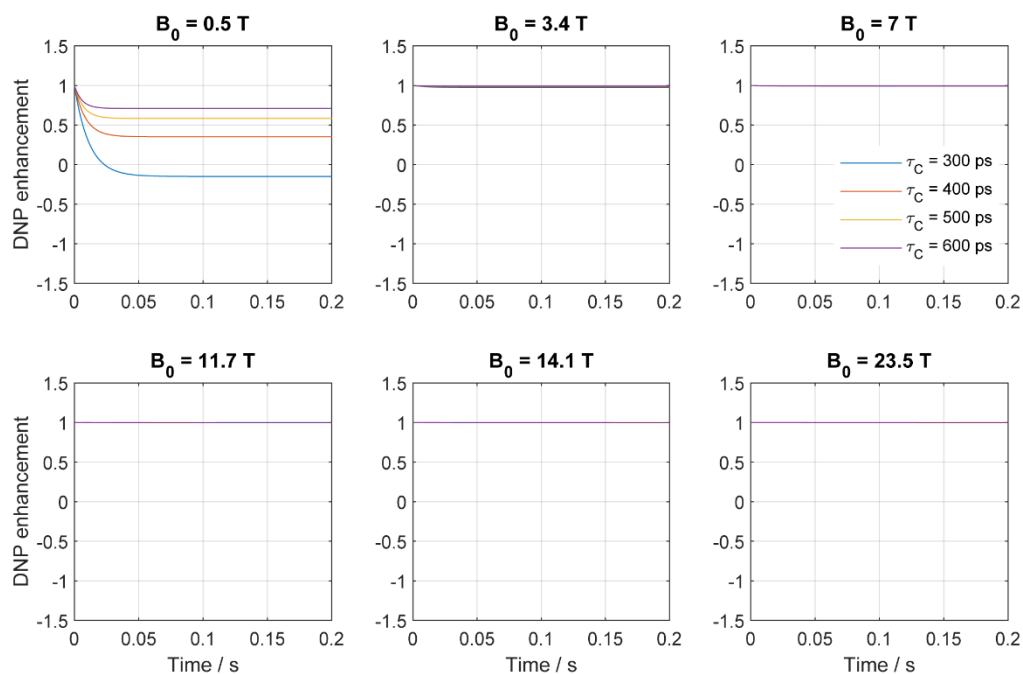


Fig. S12: Time domain simulations showing the evolution of the transient J-DNP enhancement as a function of B_0 and of τ_C . For all fields J_{ex} was tuned to $\omega_E + \omega_N$, using the parameters of the system in Table 1, but with the proton placed symmetrically in the biradical's centre (i.e., at $[0 \ 0 \ 0] \text{ \AA}$).

References

1. Owenius, R., G.R. Eaton, and S.S. Eaton, *Frequency (250 MHz to 9.2 GHz) and viscosity dependence of electron spin relaxation of triarylmethyl radicals at room temperature*. Journal of Magnetic Resonance, 2005. **172**(1): p. 168.
2. Yong, L., et al., *Electron spin relaxation of triarylmethyl radicals in fluid solution*. J Magn Reson, 2001. **152**(1): p. 156.
3. Ardenkjaer-Larsen, J.H., et al., *EPR and DNP properties of certain novel single electron contrast agents intended for oximetric imaging*. Journal of Magnetic Resonance, 1998. **133**(1): p. 1.
4. Bajaj, V.S., et al., *250 GHz CW gyrotron oscillator for dynamic nuclear polarization in biological solid state NMR*. Journal of Magnetic Resonance, 2007. **189**(2): p. 251.
5. Vega, S., *Fictitious spin 1/2 operator formalism for multiple quantum NMR*. J. Chem. Phys., 1978. **68**: p. 5518.
6. Ernst, R., R.; Bodenhausen, G.; Wokaun, A. , *Principles of Nuclear Magnetic Resonance in One and Two Dimensions*. 1987: Clarendon Press (Oxford Oxfordshire and New York).
7. Pileio, G., *Singlet NMR methodology in two-spin-1/2 systems*. Prog Nucl Magn Reson Spectrosc, 2017. **98-99**: p. 1.
8. Redfield, A., *The theory of relaxation processes*, in *Advances in Magnetic and Optical Resonance*. 1965, Elsevier. p. 1.
9. Goldman, M., *Formal theory of spin--lattice relaxation*. J Magn Reson, 2001. **149**(2): p. 160.
10. Blicharski, J., *Nuclear magnetic relaxation by anisotropy of the chemical shift*. Z Naturforsch Pt A, 1972. **27**: p. 1456.